



## Review

# Recent developments in rare-earth doped materials for optoelectronics

A.J. Kenyon\*

*Department of Electronic and Electrical Engineering, University College London, Torrington Place,  
WC1E 7JE London, UK*

---

**Abstract**

Rare-earth doped materials are of crucial importance to optoelectronics, and are widely deployed in fibre amplifiers and solid-state lasers. This article summarises the present state of the art in this rapidly growing field. Recent developments in the areas of rare-earth doped semiconductors and insulators are discussed and new classes of materials that open up new possibilities for extended functionality and greater optoelectronic integration are described. Nanostructured materials and wide bandgap semiconductors are of particular interest, though recent developments in more traditional material systems are highlighted. Emphasis is placed on erbium-doped materials, as these are of the greatest importance for telecommunications applications, but a range of other rare-earth ions are also discussed.

© 2002 Elsevier Science Ltd. All rights reserved.

*PACS:* 76.30.Kg

*Keywords:* Rare-earth doped materials; Optoelectronics; Erbium; Semiconductors

---

**Contents**

1. Introduction . . . . .	227
1.1. General background and technological perspectives . . . . .	227
2. Rare-earth luminescence in solid hosts . . . . .	231
2.1. General . . . . .	231

---

\*Corresponding author. Tel.: +44-171-419-3270; fax: +44-171-387-4350.

*E-mail address:* t.kenyon@ee.ucl.ac.uk (A.J. Kenyon).

2.1.1.	Symmetry considerations . . . . .	235
2.1.2.	Term symbols . . . . .	235
2.1.3.	Judd–Ofeldt theory . . . . .	235
2.2.	Limiting factors . . . . .	236
2.2.1.	Solubility in solid hosts . . . . .	236
2.2.2.	Phonon interactions . . . . .	236
2.2.3.	Ion–ion interactions . . . . .	237
2.2.3.1.	Co-operative upconversion . . . . .	238
2.2.3.2.	Energy migration . . . . .	240
2.2.3.3.	Cross relaxation . . . . .	240
2.2.4.	Excited state absorption . . . . .	240
3.	Rare-earth ions in semiconductors . . . . .	241
3.1.	Silicon . . . . .	241
3.1.1.	Crystalline silicon . . . . .	242
3.1.2.	Amorphous silicon . . . . .	248
3.1.3.	Porous silicon . . . . .	248
3.1.4.	Nanocrystalline silicon . . . . .	250
3.1.5.	Silicon resonating structures . . . . .	250
3.1.6.	SiGe . . . . .	252
3.2.	Gallium arsenide and other III–V hosts . . . . .	253
3.3.	Wide bandgap semiconductors . . . . .	255
3.3.1.	Gallium nitride . . . . .	255
3.3.2.	Silicon carbide . . . . .	260
4.	Rare-earth ions in insulators . . . . .	260
4.1.	Silica . . . . .	260
4.1.1.	Fibres . . . . .	261
4.1.2.	Waveguides . . . . .	263
4.2.	Silicon-rich silica . . . . .	264
4.3.	Alumina . . . . .	268
4.4.	Lithium niobate . . . . .	269
4.5.	Low phonon hosts . . . . .	270
4.5.1.	Fluorides . . . . .	271
4.5.2.	Chalcogenides . . . . .	273
4.5.3.	Tellurites . . . . .	274
5.	Rare-earth ions in polymers and organic hosts . . . . .	275
6.	Future prospects . . . . .	276
	References . . . . .	278

## 1. Introduction

### 1.1. General background and technological perspectives

The field of luminescence from rare-earth ions has been one of steady growth during the past decade, principally due to the ever-increasing demand for optical sources and amplifiers operating at wavelengths compatible with fibre communications technology. In particular, there has been enormous demand for sources that can be readily integrated with existing fibre and/or silicon microelectronics technology, and in this context rare-earth doping of silica and silicon have been areas of particular importance. The fortunate coincidence between the  $\text{Er}^{3+}$  emission band around 1535 nm and the principal low-loss window in the absorption spectrum of aluminosilicate optical fibre has been the main driving force behind much recent work on erbium-doped materials; in particular, silica optical fibres and waveguides. However, the technological interest in rare-earth luminescence reaches beyond telecommunications: displays, laser materials, data storage, radiation detection, and medical applications are all areas in which luminescent rare earths are playing an increasingly important role. A recent article also demonstrates that not only is rare-earth luminescence in itself technologically important, but it can also be used as a valuable diagnostic tool to probe the physical and optical properties of a range of optoelectronic materials [1].

Rare-earth ion luminescence is by no means a new field; sharp luminescence bands from the lanthanides have been known since the beginning of the 20th century. The energy levels of the lanthanide ions in a range of crystals were extensively investigated and tabulated by Dieke and co-workers in 1968 [2], and the rare earths have been widely used as the active ions in phosphors for several decades. The most common CRT phosphors exploit the visible transitions of the triply charged ions of erbium ( $\text{Er}^{3+}$ ), europium ( $\text{Eu}^{3+}$ ), terbium ( $\text{Tb}^{3+}$ ) and cerium ( $\text{Ce}^{3+}$ ) to produce the saturated red, green and blue required for full colour display. There is therefore a substantial body of work on the use of rare-earth ions as phosphor activators, and this is a mature technology. Moving on from this, chronologically speaking, much research in the 1960s was concerned with the development of solid-state lasers exploiting the luminescence of rare-earth ions in glasses and crystals. The Nd:YAG laser is perhaps the most notable success from this period, and there is continued interest in novel rare-earth doped materials for lasers. Nd:glass lasers are widely used in very high power applications such as fusion research, and other rare earths such as holmium and praseodymium have found uses in fibre lasers and lasers for medical applications. More recently, however, optoelectronics has emerged as the principal area of research into rare-earth luminescence, and the present article therefore concentrates on the variety of different ways in which rare-earth luminescence has been exploited in this field. This covers such applications as telecommunications (long-haul and local area networks), chip-to-chip and on-chip interconnects, optical memories, and the direct integration of display technology with silicon and other semiconducting materials. Phosphors are specifically excluded, although there is much interest in producing novel phosphors for use in LCD and

field emission displays, because this area is broad enough to warrant separate treatment.

In recent years most of the interest in luminescent rare-earth ions has concentrated on one species: trivalent erbium ( $\text{Er}^{3+}$ ), and in particular its emission band around  $1.53\ \mu\text{m}$ . The reasons for this are plain to see if one considers the rapid growth in optical telecommunications and some of the materials limitations on this technology. The loss spectrum of silica fibre (Fig. 1) has two low loss “windows”: one between 1200 and 1350 nm, and a second (termed the “ultra low-loss window”) around 1450–1600 nm. These are produced by the combined effects of losses due to Rayleigh scattering, overtones of the hydroxyl absorption, and infrared absorption due to the Si–O species. The 1500 nm window is the wavelength region of choice for telecommunications, and fortuitously coincides with the  $1535\ \text{nm}$  intra-4f  ${}^4\text{I}_{13/2} \rightarrow {}^4\text{I}_{15/2}$  transition of the  $\text{Er}^{3+}$  ion (Fig. 2). For this reason there has been intense interest in utilising erbium-doped materials for gain elements and sources in telecommunications systems. The development of the erbium-doped fibre amplifier (EDFA) in the late 1980s [3,4] exploited the  ${}^4\text{I}_{13/2} \rightarrow {}^4\text{I}_{15/2}$  transition and allowed the transmission and amplification of signals in the  $1530\text{--}1560\ \text{nm}$  region without the necessity for expensive optical to electrical conversion [5]. It offered several advantages over electrical amplification, including the capability to produce gain at many different wavelengths simultaneously; a key requirement for wavelength division multiplexing (WDM). The silica EDFA has been a tremendous success

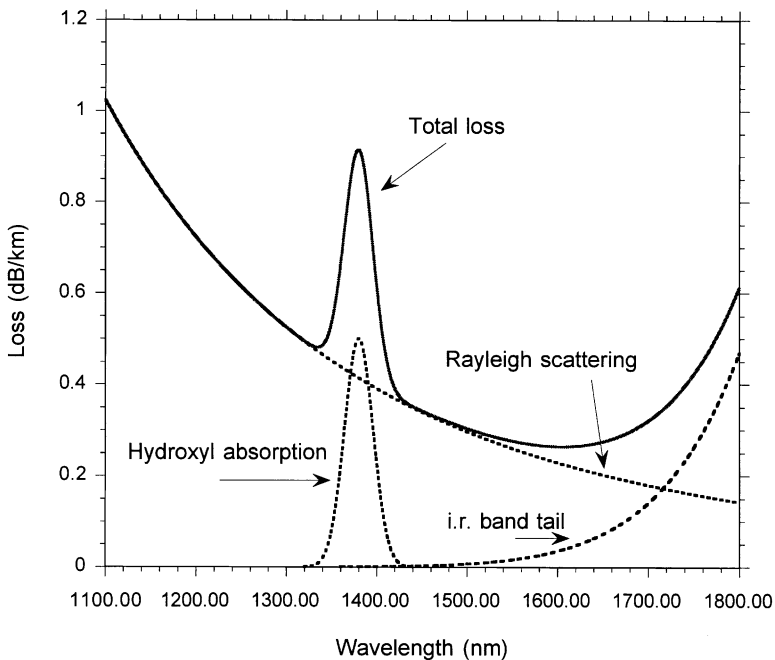


Fig. 1. Loss spectrum of silica optical fibre in the near-IR region.

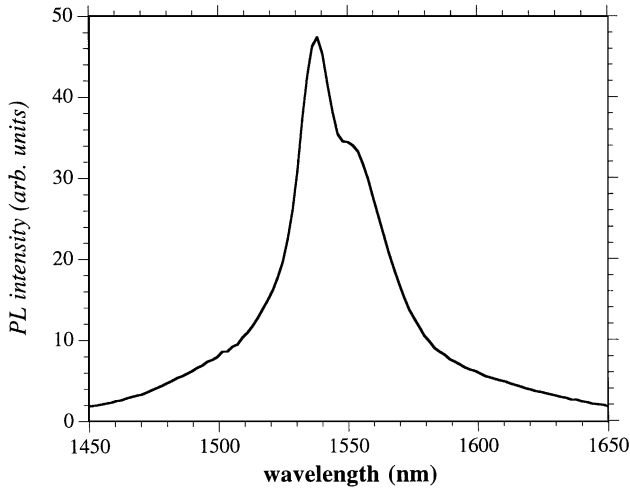


Fig. 2. Photoluminescence spectrum of the  ${}^4I_{13/2}$  to  ${}^4I_{15/2}$   $\text{Er}^{3+}$  transition in a silica host.

story, has been widely deployed in long-haul telecommunications links, and the technology is still developing at a rapid pace as larger and larger bandwidths are demanded. Novel hosts and a careful choice of amplifier design and pumping configuration have produced amplifiers with broad and flat gain profiles across much of the 1500 nm window, and this remains an active field of research and development. However, there is also a growing interest, fuelled by the same demand for increased bandwidth, in extending the spectral range of fibre amplifiers and associated sources using other luminescent rare-earth ions and novel hosts. A key development in this respect has been the production of very low hydroxyl fibres, which have a negligible  $-\text{OH}$  absorption around 1.4  $\mu\text{m}$ . Such materials have opened up the potential bandwidth available for WDM applications and have driven much of the research into rare-earth doped materials exhibiting gain around 1.4  $\mu\text{m}$ .

Erbium has also dominated research into light emission from other solid hosts, most notably semiconductors, and in particular, silicon (Table 1). Electroluminescence at 1.5  $\mu\text{m}$  from erbium-doped LEDs has been demonstrated in a number of semiconductor systems, including Si, SiC, GaAs, GaP, and, more recently, GaN. Early work concentrated on III–V materials such as InP and GaAs, though the appeal of integration with silicon microelectronics has driven the Er:Si research to become the area within which the majority of the rare-earth doped semiconductor research is performed. As an indication of the continuing and growing interest in this field, the reader is directed to the proceedings of recent symposia on rare-earth doped materials and devices [6,7] and rare-earth doped semiconductors (see articles in Ref. [8]).

This article is arranged by host material. It is broadly divided into semiconductors and insulators, and then further subdivided into more specific material systems. In most cases this results in a reasonable correspondence with application. Rare-earth

Table 1  
Optical parameters of  $\text{Er}^{3+}$  in a range of host materials

	Peak absorption cross-section (488 nm)	Peak absorption cross-section (980 nm)	${}^4\text{I}_{13/2} \rightarrow {}^4\text{I}_{15/2}$ PL lifetime <sup>a</sup>	Upconversion coefficient	Peak-stimulated emission cross-section (1535 nm)	Luminescence bandwidth (1535 nm FWHM at 300 K)	Maximum optically active concentration
Silica [19]	$< 8.0 \times 10^{-21} \text{ cm}^2$	$1.0 \times 10^{-21} \text{ cm}^2$	$12 \times 10^{-3} \text{ s}$	$3.0 \times 10^{-21} \text{ cm}^2$	$7.27 \times 10^{-21} \text{ cm}^2$	11 nm	0.1 at% (melt glass) (PECVD)
Phosphosilicate glass [19]		$2.01 \times 10^{-21} \text{ cm}^2$	$10 \times 10^{-3} \text{ s}$	$9.0 \times 10^{-21} \text{ cm}^3 \text{ s}^{-1}$		27 nm	2.5 at%
Aluminosilicate glass [19,126]		$3.12 \times 10^{-21} \text{ cm}^2$	$10 \times 10^{-3} \text{ s}$	$1.0 \times 10^{-16} \text{ cm}^3 \text{ s}^{-1}$	$5.7 \times 10^{-21} \text{ cm}^2$	43 nm	500 ppm
Silicon (crystalline) [19]	$2.8 \times 10^{-12} \text{ cm}^2$ (514 nm)		$420 \times 10^{-6} \text{ s}$				$3 \times 10^{17} \text{ cm}^{-3}$
Amorphous silicon [19]	$1.4 \times 10^{-14} \text{ cm}^2$ (514 nm)		$800 \times 10^{-6} \text{ s}$				
Silicon-rich silica [143]	$7.3 \times 10^{-17} \text{ cm}^2$	—	$\sim 2.5 \times 10^{-3} \text{ s}$ (depends on Si content)			Up to 60 nm (depends on Si content)	—
Porous silicon [60]						–10 nm	
Alumina [19,191]		$2.0 \times 10^{-21} \text{ cm}^2$	$1 \times 10^{-3} \text{ s}$	$4.0 \times 10^{-18} \text{ cm}^3 \text{ s}^{-1}$	$6.0 \times 10^{-21} \text{ cm}^2$	55 nm	
GaN [120,114]		$4.8 \times 10^{-21} \text{ cm}^2$	$7.8 \times 10^{-3} \text{ s}$			~8 nm	
GaAs			$2.95 \times 10^{-3} \text{ s}$				
ZBLAN [172]			$1 \times 10^{-3} \text{ s}$		$1 \times 10^{-3} \text{ cm}^2$		$7 \times 10^{17} \text{ cm}^{-3}$
Lithium niobate [19]			$3.0 \times 10^{-3} \text{ s}$	$< 1.4 \times 10^{-19} \text{ cm}^3 \text{ s}^{-1}$	$5.0 \times 10^{-21} \text{ cm}^2$		18 mol%
YAG			$0.8 \times 10^{-6} \text{ s}$	$5.4 \times 10^{-17} \text{ cm}^3 \text{ s}^{-1}$		70 nm	
PPMA [206]	$1.1 \times 10^{-20} \text{ cm}^2$		$3.3 \times 10^{-3} \text{ s}$			80 nm	
Tellurite [194,193,190,197]		$4.48 \times 10^{-21} \text{ cm}^2$		$2.74 \times 10^{-17} \text{ cm}^3 \text{ s}^{-1}$	$1.3 \times 10^{-20} \text{ cm}^{-2}$		2.5 at%

<sup>a</sup>Maximum value reported in unclustered material.

doped silicon is therefore of most interest for the production of fully integrated emission sources and drive electronics for local area telecommunications, along with optical communication within and between chips. Rare-earth doped glasses are predominantly used to produce fibre- or waveguide-based gain elements for longer haul communications, or perhaps for laser sources. Rare-earth doped wide-bandgap semiconductors are principally, though not wholly, of interest for visible emission. In all cases, the rare-earth ion can serve as a sensitive probe of the electronic and structural properties of the host material.

## 2. Rare-earth luminescence in solid hosts

### 2.1. General

The rare earths, otherwise referred to as the lanthanides, comprise the series of elements in the sixth row of the periodic table stretching from lanthanum to ytterbium. They are characterised by a partially filled 4f shell that is shielded from external fields by  $5s^2$  and  $5p^6$  electrons. The energy levels of elements in this series are therefore largely insensitive to the environment in which they are placed. When incorporated in crystalline or amorphous hosts, the rare earths exist as  $3^+$ , or occasionally  $2^+$ , ions. The  $3^+$  ions all exhibit intense narrow-band intra-4f luminescence in a wide variety of hosts, and the shielding provided by the  $5s^2$  and  $5p^6$  electrons means that rare-earth radiative transitions in solid hosts resemble those of the free ions and electron–phonon coupling is weak. Although some of the divalent species also exhibit luminescence (principally samarium and europium), it is the trivalent ions that are of most interest.

As a result of the shielding of the 4f electrons, the positions of rare-earth electronic levels are influenced much more by spin–orbit interactions than by the applied crystal field. The intra-4f transitions are parity forbidden and are made partially allowed by crystal field interactions mixing opposite parity wavefunctions. Luminescence lifetimes are therefore long (often in the millisecond range), and linewidths narrow. By careful selection of the appropriate ion, intense, narrow-band emission can be obtained across much of the visible region and into the near-infrared. Fig. 3 shows energy level diagrams for the isolated  $3^+$  ions of each of the 13 lanthanides with partially filled 4f orbitals from cerium ( $n = 1$ ) to ytterbium ( $n = 13$ ). The most technologically important radiative transitions are labelled. Fig. 4 further illustrates the effect of spin–orbit and crystal field interactions on the energy levels of the  $Er^{3+}$  ion.

A number of excitation pathways are available for rare-earth luminescence in solid hosts. These can be broadly classified as either direct or indirect mechanisms. Amongst the former are resonant optical excitation by the interaction of photons of appropriate wavelengths with specific rare-earth 4f absorption bands, cathodoluminescence, and electroluminescence in semiconductor hosts involving hot electron collision with rare-earth centres. Indirect mechanisms include carrier-mediated excitation transfer in semiconductors, and dipole–dipole Förster–Dexter coupling in

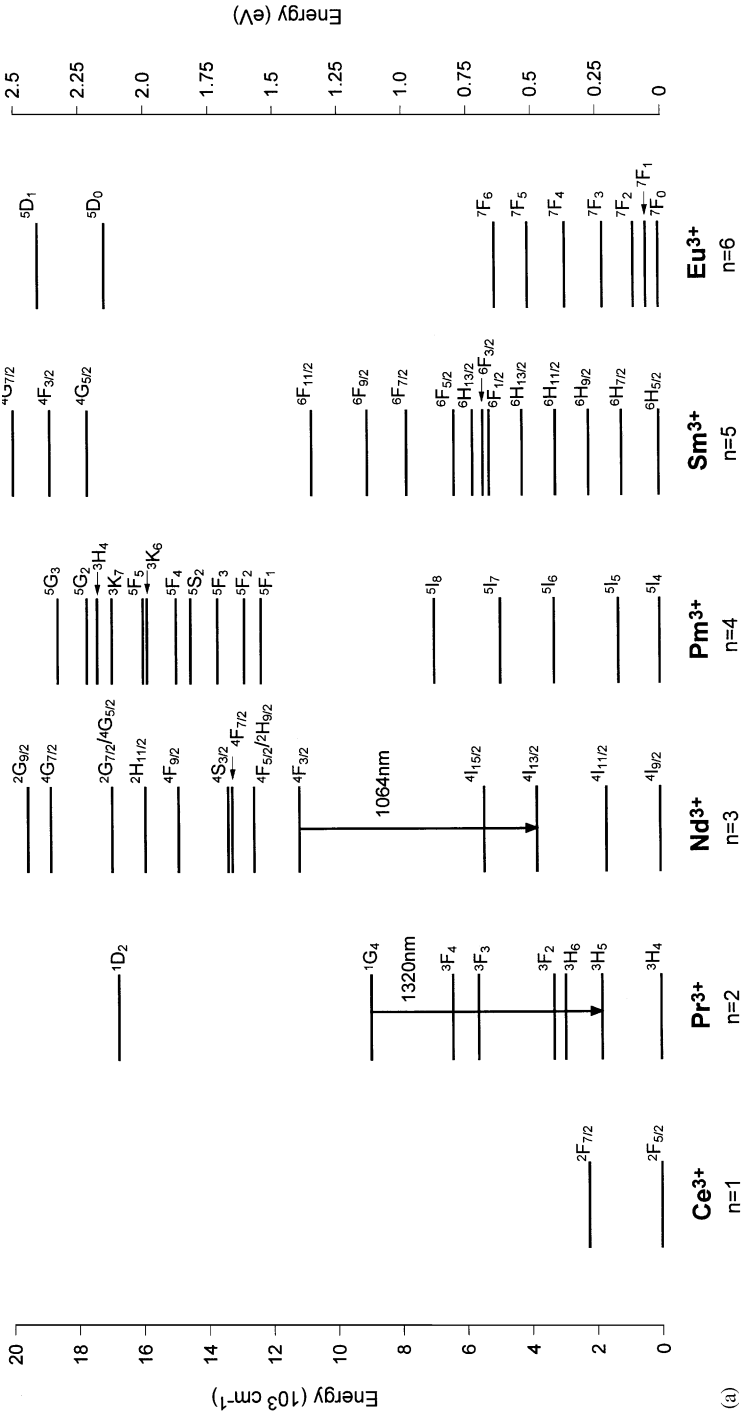


Fig. 3. Energy levels of the triply charged lanthanide ions. The most technologically important radiative transitions are labelled.

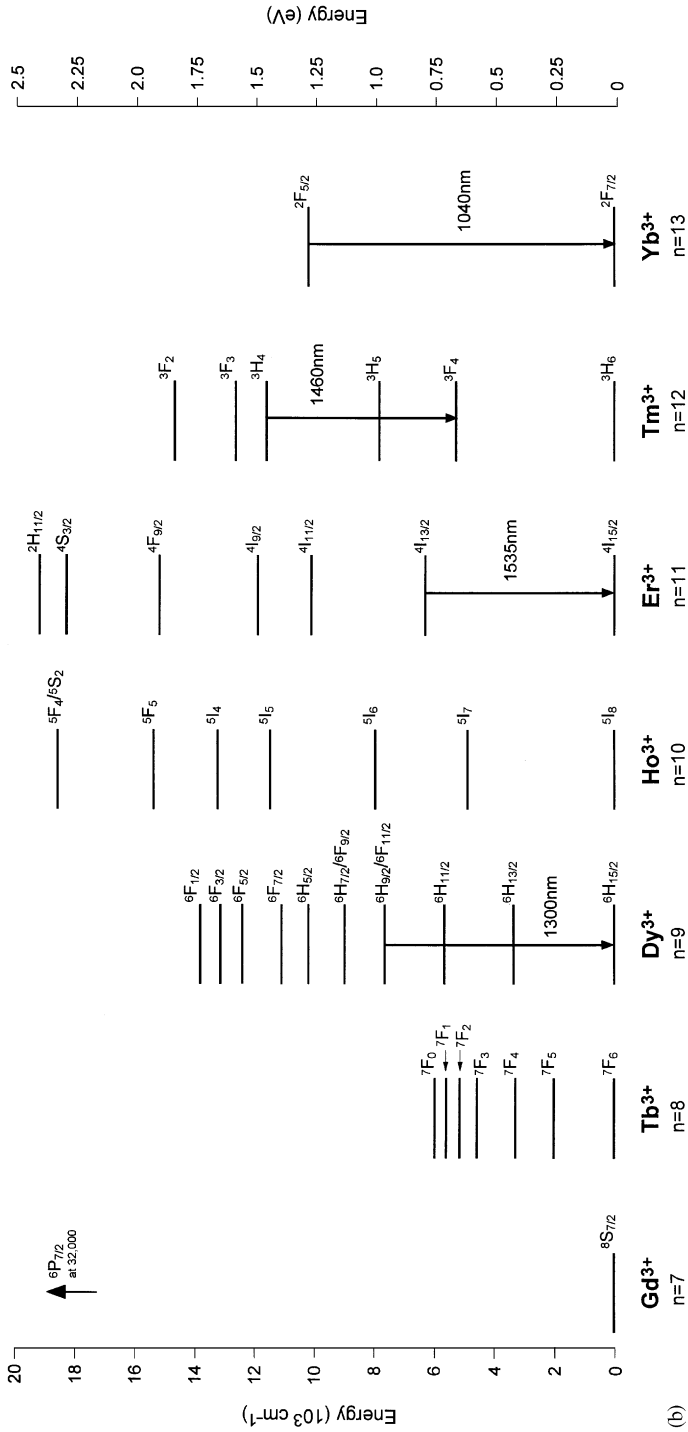


Fig. 3 (continued).

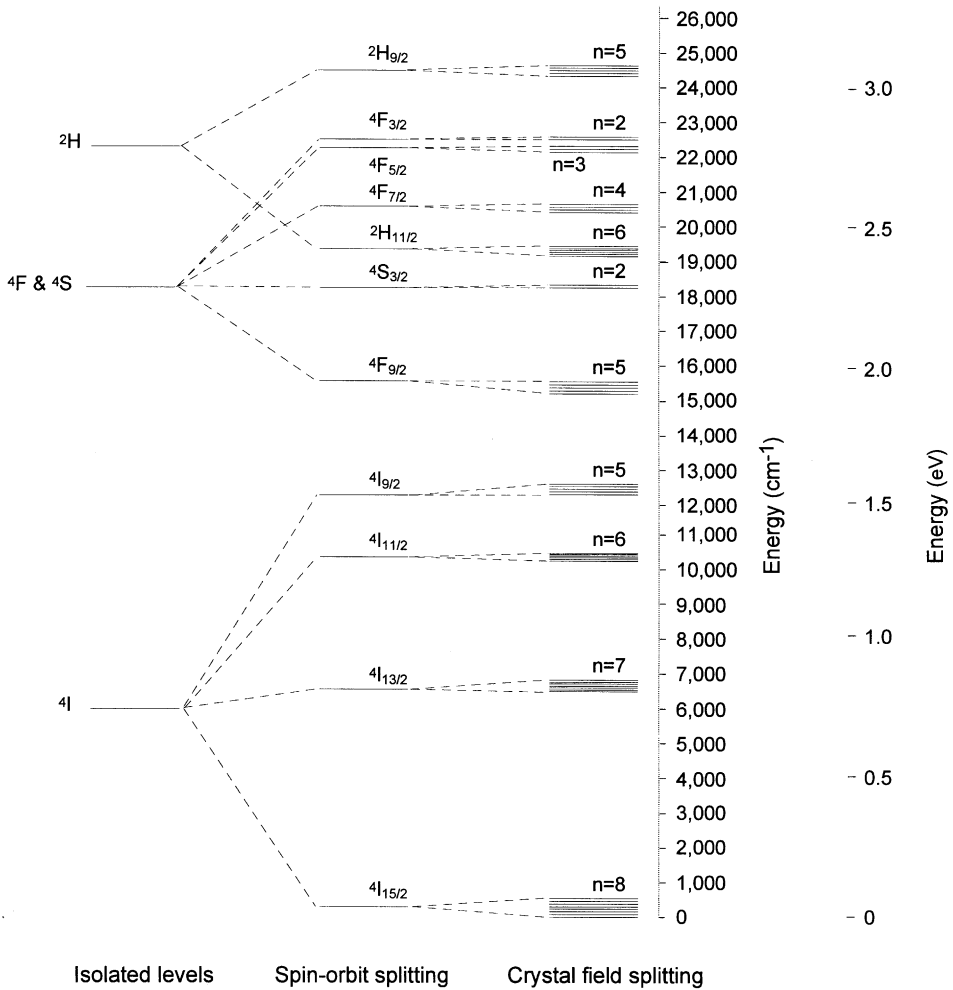


Fig. 4. The effect of spin-orbit and crystal field splitting on the energy levels of the  $\text{Er}^{3+}$  ion in silica.

insulators. Carrier-mediated excitation is of particular importance for the production of optoelectronic devices, and there has been much work directed at an understanding of such processes in a range of semiconductor hosts. It is generally thought that rare earths in semiconductors (particularly III–V compounds) occupy isoelectronic substitutional sites (see below). Such sites constitute trap centres in which there is a strong interaction between free carriers and the partially filled 4f shell of the rare-earth ion. Although the details of their structure remain poorly understood, rare-earth traps have relatively large carrier capture cross-sections, and readily form bound excitons through Coulombic interaction between trapped and free carriers. Energy transfer from the bound carriers to the rare-earth 4f shell may

then proceed either by inelastic scattering or excitonic recombination. Since carrier-mediated excitation produces ions in high-lying excited states, phonon coupling is usually required to enable rapid de-excitation to lower radiative levels. Thus, for example, in gallium nitride  $\text{Er}^{3+}$  is promoted by interaction with free carriers to the  $^2\text{H}_{9/2}$ ,  $^4\text{F}_{3/2}$ , or  $^4\text{F}_{7/2}$  manifolds, from which non-radiative phonon-assisted relaxation to either the  $^2\text{H}_{11/2}$  or  $^4\text{S}_{3/2}$  levels produces emission at 523 and 546 nm, respectively, due to transitions to the  $^4\text{I}_{15/2}$  ground state (see below).

### 2.1.1. Symmetry considerations

A key question in much of the work on rare-earth ions in solid hosts is what is the specific site occupied by the ion. In some cases it is relatively straightforward to determine unambiguously (for example, in GaN,  $\text{Er}^{3+}$  occupies a substituted Ga site with  $\text{C}_{3v}$  symmetry), but in general the picture can be somewhat confused. Assignment of site symmetry from a study of low temperature intra-4f luminescence is problematic and ambiguous thanks to vibronic splittings, contributions from mixed symmetries and splitting of crystal field levels. Luminescence studies must be combined with ESR, polarisation, Zeeman, and point-charge calculation techniques for the full identification of rare-earth sites. Theoretical studies employing first-principles molecular orbital calculations have been performed in a small number of cases, though these procedures tend to be lengthy and verification with experimental results is difficult.

Although shielding of the 4f shell means that the rare-earth ion energy levels are largely independent of host, Stark splitting broadens the levels as a result of the applied crystal field. Full Stark splitting is observed for rare-earth ions in glasses, as a result of the low point symmetries of the rare-earth sites in amorphous matrices [9,10]. For example,  $\text{Er}^{3+}$  ions in silica exhibit  $(2J+1)/2$  Stark levels due to splitting of the  $J$  manifold, which leads to a total of 56 possible  $^4\text{I}_{13/2}$  to  $^4\text{I}_{15/2}$  transitions. However, these levels may only be resolved in emission spectra of crystalline hosts taken at low temperature, and at room temperature the Stark levels broaden and overlap to produce an inhomogeneously broadened emission band.

### 2.1.2. Term symbols

Energy levels in rare-earth ions are conventionally labelled according to their angular momentum and spin quantum numbers using term symbols such as  $^4\text{I}_{13/2}$ , or  $^2\text{F}_{7/2}$ . Here the letter refers to the total orbital angular momentum of the ion obtained by combining the orbital angular momenta of the individual electrons in the ion according to the Clebsch–Gordan series. The left superscript is the number of possible orientations of the total spin of the ion, given as  $2S+1$ , where  $S$  is the total spin of the ion. The right subscript gives the total angular momentum of the ion and is determined using the Russell–Saunders coupling scheme [11].

### 2.1.3. Judd–Ofeldt theory

It is important to know the transition probabilities, or oscillator strengths, for the various transitions between energy levels in rare-earth ions. Unfortunately, these are extremely difficult to measure, and instead must be calculated using Judd–Ofeldt

theory [12–14]. This states that the oscillator strength for the transition between two states  $^{2S+1}L_J$  (described by the wavefunction  $\Psi_i$ , specified by the  $f^N$  configuration for a partially filled f shell, the quantum numbers  $S$ ,  $L$ , and  $J$ , and a factor  $\gamma$  to distinguish electronic states that share the same values of  $S$  and  $L$ ) and  $^{2S+1}L'_J$  ( $\Psi_{if}$ , specified in a similar way) is given by

$$S = \frac{1}{e^2} |\langle \Psi_f | H | \Psi_i \rangle|^2 = \sum_{k=2,4,6} \Omega_k |\langle f^N \gamma S' L' J' | U^{(k)} | f^N \gamma S L J \rangle|^2.$$

Here  $H$  is the electric dipole Hamiltonian, expressed in tensor form as  $U^{(k)}$ , and the  $\Omega_k$  coefficients are the Judd–Ofeldt parameters. Physically, these may be considered as a set of coefficients describing the influence of the external crystal field on the radiative transition probabilities of the intra-4f transitions. Tables of the Judd–Ofeldt parameters are readily available for most hosts.

## 2.2. Limiting factors

### 2.2.1. Solubility in solid hosts

Beyond critical concentrations, rare-earth ions tend to form precipitates in most solid hosts. These can either take the form of clusters of rare-earth ions, as in the often macroscopic rare-earth aggregates observed in Er-doped silica, or can be compounds or alloys formed with one component of the host matrix. Thus, erbium arsenide precipitates can be formed at high Er concentrations in erbium-doped gallium arsenide. Such aggregates serve to quench luminescence, either by increasing ion–ion interactions between rare-earth ions or groups of ions (see below), or by forming rare-earth compounds that are not optically active. Upper limits are therefore placed on rare-earth concentrations in solid hosts that can range from around  $7 \times 10^{17} \text{ cm}^{-3}$  in GaAs to several atomic percent in some fluoride glasses or gallium lanthanum sulphides. This places clear technological limitations on the production of, for example, erbium-doped silica fibre amplifiers, for which reason such devices typically contain several metres of lightly doped fibre in order to achieve sufficient gain (see below).

### 2.2.2. Phonon interactions

Multiphonon relaxation can rapidly depopulate the upper excited state and therefore readily quench luminescence [15]. Such processes only occur when a small number of phonons are required to bridge the energy gap between the upper and lower electronic states of the rare-earth ion. As a guide, it is generally held that if the phonon cut-off energy of the matrix is greater than 25% of the energy gap ( $\Delta E$ ), rare-earth luminescence will be completely quenched. For phonon cut-off energies between 10% and 25% of  $\Delta E$ , quenching will result in a temperature-dependent luminescence lifetime, whilst for phonon cut-off energies smaller than this the contribution of multiphonon relaxation will be negligible [16]. The importance of multiphonon processes therefore depends strongly on both the host material and the electronic structure of the rare earth. In the case of erbium, the energy gap of the  $^4I_{13/2}$  to  $^4I_{15/2}$  transition is approximately  $6500 \text{ cm}^{-1}$ . The phonon cut-off energy of

silica is  $1100\text{ cm}^{-1}$ , and therefore the rare-earth luminescence at 1535 nm is only weakly quenched at room temperature in silica. Selection of lower phonon hosts such as fluoride or tellurite glasses can reduce the contribution of multiphonon relaxation and allow radiative transitions that would otherwise be quenched (for example, the  $2.7\text{ }\mu\text{m}$   ${}^4\text{I}_{11/2}$  to  ${}^4\text{I}_{13/2}$  transition in erbium). It should be noted that in all glass hosts other than fluorides, all transitions in erbium are non-radiative with the exception of the  ${}^4\text{I}_{13/2}$  to  ${}^4\text{I}_{15/2}$  transition. Thus, for example, the non-radiative decay rate for the  ${}^4\text{I}_{11/2}$  to  ${}^4\text{I}_{13/2}$  transition in silica is around  $1.5 \times 10^5\text{ s}^{-1}$ , whilst that for the  ${}^4\text{I}_{13/2}$  to  ${}^4\text{I}_{15/2}$  transition in the same matrix is essentially zero.

### 2.2.3. Ion–ion interactions

A characteristic of the rare-earth ions is their tendency to ion–ion interactions [15]. These can either be between ions of the same rare earth (as is the case in clustered material), or between different ions (as in the sensitisation of one rare-earth ion by another). The former constitutes a loss mechanism, increasing non-radiative decay channels or luminescence from unwanted transitions. The latter can be employed in novel pumping schemes whereby excitation is provided to one species and transferred to another, allowing a wider selection of pump sources to be used. Examples of such mechanisms are the Er/Yb codoping schemes adopted in alumina or silica to increase the luminescence efficiency of the  $\text{Er}^{3+}$  ion by coupling to the absorption bands of the Yb codopant. Introducing a second rare-earth dopant can also provide the added bonus of inhibiting aggregation of the emitting species through the formation of a solvation shell.

Ion–ion interactions due to multipolar interactions between neighbouring rare-earth ions have been studied for some time; the first detailed treatment being that due to Forster [17] and Dexter [18]. In this model, two nearby ions are labelled as donor (D) and acceptor (A), respectively. The donor is that ion that is in the excited state, and the acceptor is that ion that is initially unexcited. Note that the two ions need not necessarily be both of the same rare earth.

A donor to acceptor transfer efficiency may be defined as

$$\eta_{\text{D}} = \frac{W_{\text{DA}}\tau_{\text{D}}}{1 + W_{\text{DA}}\tau_{\text{D}}},$$

where  $W_{\text{DA}}$  is the rate constant for the transfer process and  $\tau_{\text{D}}$  is the radiative lifetime of the donor ion. Note that one effect of the ion–ion interaction is to reduce the observed luminescence lifetime:

$$\tau_{\text{Obs}} = \tau_{\text{D}}(1 - \eta_{\text{D}}).$$

Dexter theory assumes an interacting ion pair, and integrating over all such pairs in a macroscopic sample, we have

$$\bar{\eta}_{\text{D}} = \int_0^{\infty} \eta_{\text{D}} P(A) dV,$$

where  $P(A)$  represents the probability of finding an acceptor ion at a distance from the donor between  $R$  and  $R + \Delta R$ , and  $V$  is the interaction

volume ( $= (4\pi R^3)/3$ ):

$$P(A) dV = \rho_A (e^{-\rho_A V}),$$

where  $\rho_A$  is the acceptor density. Note further that

$$W_{DA}\tau_D = \left(\frac{1}{\rho_A V}\right)^{n/3}$$

which yields an  $I/R^n$  dependence of the strength of multipolar interactions:  $n = 6$  for dipole–dipole,  $n = 8$  for dipole–quadrupole,  $n = 10$  for quadrupole–quadrupole.

Note, however, that a more detailed description of ion–ion interactions is given by Inokuti–Hirayama theory [14], which explicitly deals with the dynamics of energy migration. A full description of this lies outside the scope of this article, but it should be noted that it predicts the same radial dependence of the ion–ion interaction and that the corrections due to this theory apply mainly to the higher-order interactions (dipole–quadrupole and quadrupole–quadrupole).

In materials containing only one rare-earth species, a number of different ion–ion interactions occur, the most important of which are outlined below. Fig. 5 illustrates each of these schematically for the case of erbium.

*2.2.3.1. Co-operative upconversion.* Ions in the metastable state decaying to the ground state can couple in such a way that the decay of ion 1 promotes nearby ion 2 into a higher level (Fig. 5(a)). Once in the higher state, ion 2 may then decay rapidly and non-radiatively, or alternatively return to the metastable state and subsequently emit light. In the case of oxide glasses, the relaxation is rapid and non-radiative, and hence the result of co-operative upconversion is to lose an excitation to heat.

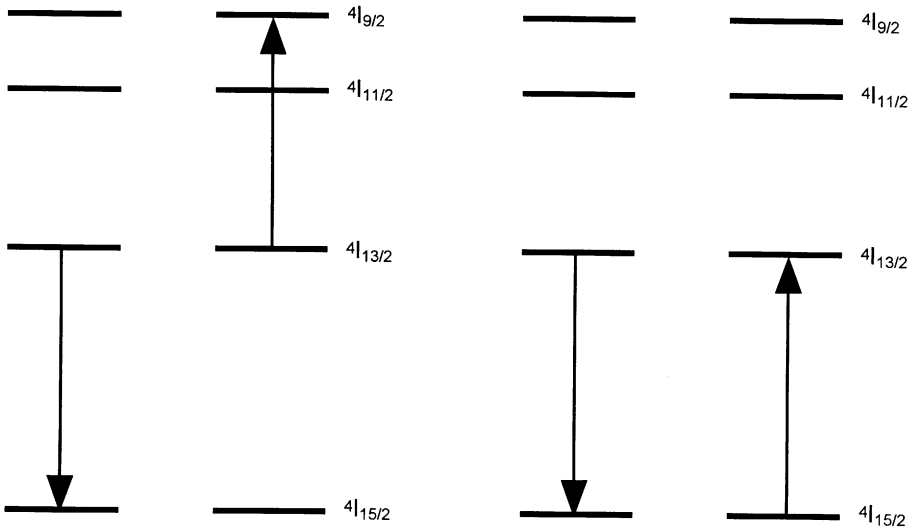
Co-operative upconversion relies on the two interacting ions being in the metastable state. Because of this, it only becomes important at high excitation levels. It is evident as a reduced metastable state lifetime at high excitation intensities, and a non-exponential luminescence decay.

In modelling this process, it is generally assumed that the lifetime of the higher excited state is very short compared to that of the metastable level, in which case a simple rate equation may be written to describe the upconversion process, and an upconversion coefficient,  $C_{up}$  defined. The higher level state in erbium ( ${}^4I_{9/2}$ ) has a lifetime in the nanosecond range: much smaller than the 10 ms lifetime of the metastable level in silica, and hence the approximation can usefully be made. Thus for erbium:

$$\frac{dn^2}{dt} = W_{1,2}n_1 - W_{2,1}n_2 - A_{2,1}n_2 - 2C_{up}n_2^2,$$

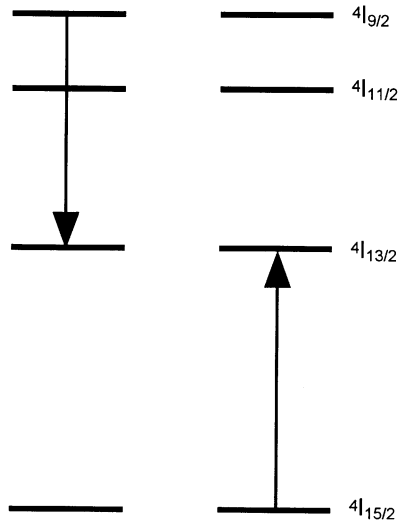
where subscripts 1 and 2 refer to the ground ( ${}^4I_{15/2}$ ) and metastable ( ${}^4I_{13/2}$ ) states, respectively; the three rate coefficients  $W_{1,2}$ ,  $W_{2,1}$ , and  $A_{2,1}$  refer to the absorption of a pump photon, stimulated emission, and spontaneous emission, respectively.

Note that the upconversion term appears as a quadratic, as two excited state ions are involved in the transition. In addition, we have treated the erbium ion as a



(a) Co-operative upconversion

(b) Energy migration



(c) Cross-relaxation

Fig. 5. Ion-ion interactions between two neighbouring  $\text{Er}^{3+}$  ions.

quasi-two-level system in which the  ${}^4\text{I}_{9/2}$  lifetime is sufficiently short to enable the following approximation to be made:

$$[\text{Er}] = n_1 + n_2.$$

Thus the upconversion process is strongly dependent on the erbium concentration in addition to the excitation intensity.

**2.2.3.2. Energy migration.** An ion in the metastable state can interact with a nearby ground state ion, promoting it to the  ${}^4\text{I}_{13/2}$  level (Fig. 5(b)). Although radiative emission may still occur from the second ion, the probability of non-radiative decay is increased with each successive transfer, and hence this constitutes a loss mechanism. Dipole–dipole Förster–Dexter interactions are responsible for this process, and therefore energy migration is again strongly dependent on rare-earth ion concentration.

**2.2.3.3. Cross relaxation.** This is the process whereby excitation energy from an ion decaying from a highly excited state promotes a nearby ion from the ground state to the metastable level. In erbium, the energy gap between the  ${}^4\text{I}_{9/2}$  and  ${}^4\text{I}_{13/2}$  levels is close to that between the  ${}^4\text{I}_{13/2}$  and  ${}^4\text{I}_{15/2}$  levels. As a result, at sufficiently high erbium concentrations, the population of the metastable state may be increased by the decay of an ion from the  ${}^4\text{I}_{9/2}$  level and the consequent promotion of a nearby ion from the ground state (Fig. 5(c)).

#### 2.2.4. Excited state absorption

Given a sufficiently long upper state lifetime, interaction with photons of the appropriate wavelength can promote electrons in the excited state to higher lying levels resonant with the incident photon energy. An ion can therefore be promoted to higher lying electronic levels from which it may return to the metastable state by multiphonon relaxation or radiative decay. However, in the process one of the two absorbed photons has been “lost” as either heat or emission at a different wavelength from the metastable-to-ground state transition. For the purposes of optical amplification, therefore, excited state absorption constitutes a loss mechanism: two photons are absorbed with only one emitted, and much research is therefore directed at minimising it.

Because optical transitions involving ions in the excited state originate from a level other than the ground state, the absorption spectrum of excited state ions is very different from that of those in the ground state. Energy gaps are in this case relative to the excited level rather than the ground state. Fig. 6 illustrates this for  $\text{Er}^{3+}$  by tabulating the major absorption bands originating on both the  ${}^4\text{I}_{15/2}$  ground state and the  ${}^4\text{I}_{13/2}$  metastable state. Note particularly the coincidence of the  ${}^4\text{I}_{9/2}$  to  ${}^4\text{I}_{13/2}$  transition at 800 nm and that at 790 nm due to the  ${}^4\text{I}_{13/2}$  to  ${}^4\text{S}_{3/2}$  transition. Excited state absorption at 800 nm depopulates the metastable state, and as a result, this is not widely used as a pump wavelength.

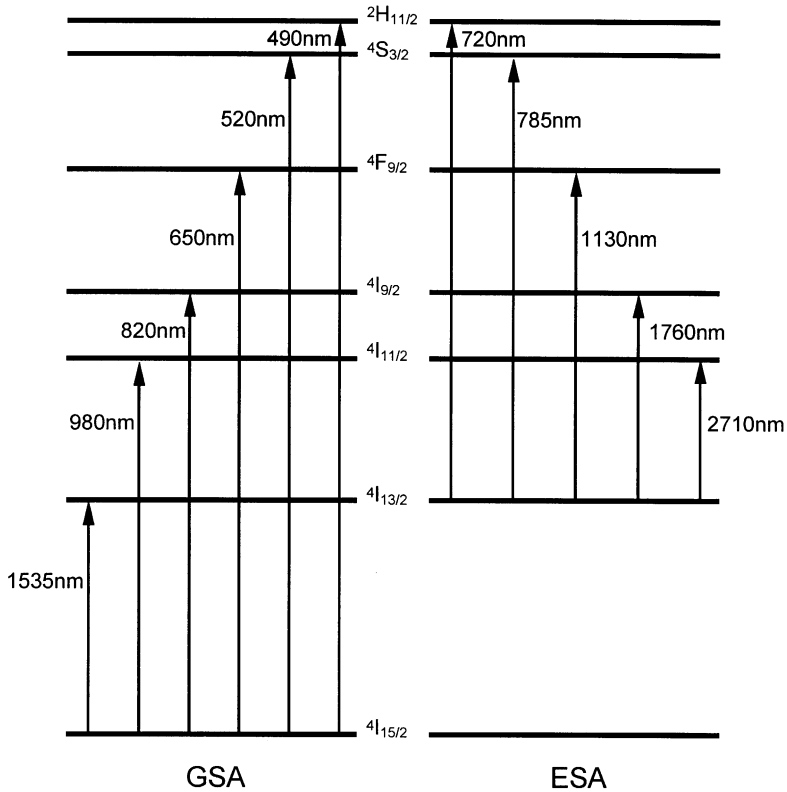


Fig. 6. Ground- and excited-state absorption transitions in erbium.

### 3. Rare-earth ions in semiconductors

A number of semiconductor systems have been studied as hosts for rare-earth ions. For obvious technological reasons, silicon has been of particular interest and importance, though recent work on gallium nitride has demonstrated that it is a promising host for ions emitting in the visible region, and therefore may find application in colour displays. Incorporation of rare-earth ions in a wide range of semiconductors remains appealing because of the possibility of integrating intense narrow-band emission directly with microelectronics processing techniques.

#### 3.1. Silicon

Silicon is the semiconductor of choice for the overwhelming majority of microelectronics, and the full integration of silicon microelectronics with optical emission would allow the realisation of low-cost, high-speed communication within circuits, between processors, or across local area networks. However, the indirect

bandgap of silicon has so far precluded such integration, and current optoelectronic technologies rely on III–V semiconductor heterostructures with all the associated processing complexity and cost. The main rare-earth ion of interest in this field is erbium, as this allows interfacing with existing telecommunications wavelengths. Generally, erbium-doped silicon is produced either by ion implantation of high-quality bulk crystalline or amorphous samples, or by such deposition techniques as molecular beam epitaxy or metalorganic chemical vapour deposition. Diffusion has also been employed, with limited success in crystalline silicon, but more readily in the case of porous silicon. Er-related trap sites in the silicon matrix act as efficient recombination centres for injected carriers, producing excited state erbium ions that decay radiatively, thereby potentially producing efficient optical emission at 1.5  $\mu\text{m}$  from silicon. However, obtaining room-temperature erbium luminescence from doped silicon is not an easy matter, principally due to the low solubility of erbium in bulk silicon and very strong non-radiative coupling between the erbium ion and the silicon host. The time constant of the non-radiative transfer mechanisms is very much shorter than that of the erbium luminescence (microseconds and milliseconds, respectively) [34]. Comprehensive reviews of this area were published by Polman in 1997 [19] and Coffa et al. in 1998 [20].

### 3.1.1. Crystalline silicon

Crystalline silicon may be readily doped with rare-earth ions by ion implantation, or occasionally by MBE growth of Si:Er. One very attractive feature of erbium in crystalline silicon is its relatively large absorption cross-section (around  $10^{-12} \text{cm}^2$ ). However, much of the advantage gained from such efficient excitation is lost thanks to the strong non-radiative de-excitation pathways that predominate in this material at room temperature. The short, and to some extent tunable, radiative lifetime of  $\text{Er}^{3+}$  in silicon (see below) is a definite advantage from the perspective of producing sources capable of rapid modulation, though the low emission efficiencies and strong temperature quenching present severe limitations on the exploitation of bulk silicon as a host material. The low solubility of the rare-earth ions in silicon is principally due to a combination of mismatch in ionic radii between the  $3^+$  ions and silicon, and the predominantly  $\text{sp}^3$  bonding of the silicon host. There is a strong tendency for erbium ions to cluster together in precipitates that provide further non-radiative de-excitation pathways, and for this reason only relatively modest concentrations of erbium can be incorporated in silicon. Much of the work in this area has therefore been concerned with overcoming these problems [19,21,22].

Both direct optical and carrier-mediated excitation mechanisms are observed in erbium-doped silicon. For optoelectronic applications, the latter is of key importance, though photoluminescence studies of the former can yield important information about the chemical environment of the erbium ion, as well as allowing measurement of absorption and emission cross-sections. The mechanism of electrical activation of erbium in silicon is complex, involving carrier generation, trapping at erbium-related trap levels, and Auger transfer [23]. The processes involved are as follows, and are illustrated schematically in Fig. 7:

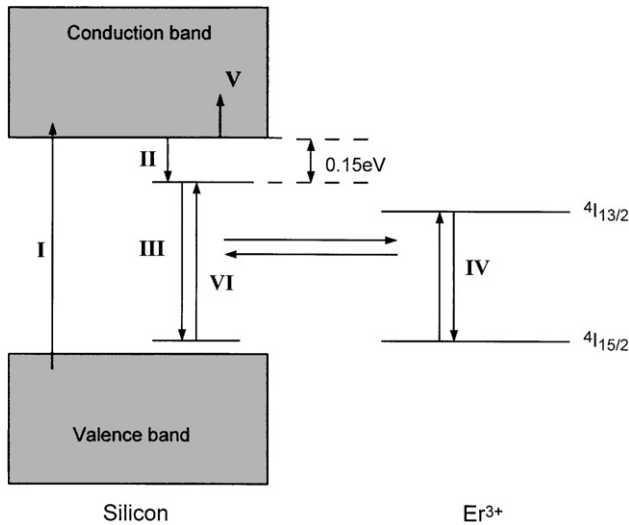


Fig. 7. Schematic representation of the interactions between  $\text{Er}^{3+}$  and crystalline silicon. See text for explanation of the labels.

- I. generation of electron–hole pairs by electrical injection;
- II. trapping of carriers at erbium-related trap centre in the silicon band gap;
- III. recombination of carriers, leading to excitation of  $\text{Er}^{3+}$  from ground state to  $^4\text{I}_{13/2}$  level;
- IV. radiative recombination of  $\text{Er}^{3+}$  with emission of  $1.5\ \mu\text{m}$  photon;
- V. non-radiative recombination of excited  $\text{Er}^{3+}$  by Auger transfer to free carriers;
- VI. de-excitation of  $\text{Er}^{3+}$ , generating bound exciton at the trap centre (“back-transfer”: the reverse of III).

The erbium-related trap levels in process II lie  $0.15\ \text{eV}$  below the silicon conduction band. Processes V and VI constitute loss mechanisms, and are responsible for the low luminescence yield of erbium in silicon at room temperature. Auger quenching is important at temperatures above  $30\ \text{K}$ , and because it is related to the concentration of free carriers in the silicon host, it is therefore proportional to the doping level. Studies by Sochoki and Langer [24] have determined that the reciprocal of the  $\text{Er}^{3+}$  luminescence decay time is proportional to the free carrier concentration according to the following formula:

$$\tau^{-1} = \frac{n}{n_0 \tau_{\text{rad}}}$$

with  $n_0$  being given by

$$n_0 = 4\pi^{5/2} n_r^{5/2} \left[ \frac{137 a_0 m_0}{m^*} \right]^{1/2} \lambda_0^{-7/2},$$

where  $n$  is the free carrier concentration,  $\lambda_0$  is the emission wavelength,  $a_0$  the Bohr radius,  $n_r$  the refractive index of the semiconductor host,  $\tau_{\text{rad}}$  the radiative lifetime, and  $m_0$  and  $m^*$  the electron rest mass and effective mass, respectively. An important consequence of this relationship is that the decay lifetime can be tailored to a specific value by changing the free carrier concentration. Above a threshold value, the decay time will be reduced below the radiative lifetime. In the case of silicon, this value has been determined by Franzó et al. [25] as  $1 \times 10^{15} \text{ cm}^{-3}$ .

Process VI (backtransfer to silicon, producing a bound exciton at the erbium-related trap) becomes significant for temperatures above 130 K, and can lead to re-excitation of the  $\text{Er}^{3+}$  ion, or non-radiative recombination of the carrier pair through phonon coupling. Measurements of luminescence intensity and decay time in p-type silicon both show a sharp decrease at temperatures above 130 K with an activation energy of 0.15 eV, corresponding to the position of the trap level below the conduction band edge. Such a small energy is easily provided by phonons, and hence the process is thermally activated. This is the process that most severely limits the room temperature performance of erbium-doped silicon LEDs, though the other side of the coin, of course, is that a problem may potentially be turned into an advantage by exploiting the backtransfer process to produce silicon-based 1.5  $\mu\text{m}$  photo-detectors. Some reports have suggested that erbium-doped pn junctions may indeed exhibit a photoresponse around 1535 nm [23], though most of the activity in this field is directed towards the production of sources.

The rate equation governing erbium luminescence in silicon is (from Ref. [25])

$$\frac{dN_{\text{Er}}^*}{dt} = \sigma\phi(N_{\text{Er}} - N_{\text{Er}}^*) - N_{\text{Er}}^* \left[ \frac{1}{\tau_b} + \frac{n}{\tau_{\text{rad}}n_0} + \frac{1}{\tau_0} \right],$$

where  $N_{\text{Er}}^*$  is the population of erbium ions in the metastable state,  $N_{\text{Er}}$  is the concentration of erbium ions,  $\sigma$  is the carrier-mediated excitation cross-section,  $\phi$  is the carrier (or photon for photoluminescence) flux density,  $\tau_b$  the backtransfer time,  $\tau_0$  the lifetime of the Er ion at temperatures below 15 K,  $n_0$  is defined as before and  $n$  is the free carrier (electron) concentration. The steady-state solution of this yields

$$N_{\text{Er}}^* = \frac{\sigma\phi\tau}{\sigma\phi\tau - 1} N_{\text{Er}},$$

where  $\tau$  is an effective lifetime given, in the low photon flux regime, by

$$\frac{1}{\tau} = \frac{1}{\tau_b} + \frac{n}{\tau_{\text{rad}}n_0} + \frac{1}{\tau_0}.$$

In recent work by Polman's group [23], which quantified the transfer mechanisms outlined above, the probability of de-excitation of a given erbium ion by backtransfer to the silicon matrix in ion-implanted material has been estimated to be as high as 70%. Moreover, it was found that the backtransfer rate (process VI) exceeds the Auger quenching of Er luminescence (process V) by three orders of magnitude at room temperature ( $1.7 \times 10^6$  cf.  $1.7 \times 10^3 \text{ s}^{-1}$ ), and that both rates are nearly zero at 15 K. However, the reported external quantum efficiency for

generation of photocurrent from 1.5  $\mu\text{m}$  illumination is of the order of  $10^{-6}$  due to the small absorption cross-section of erbium at this wavelength ( $2.7 \times 10^{-20} \text{ cm}^2$ ).

Work on erbium-doped Si LEDs has demonstrated very different behaviour under forward and reverse bias [26]. Electroluminescence yield is around an order of magnitude greater in the latter; an effect attributed to impact excitation of erbium by hot carriers under reverse bias. Moreover, non-radiative processes are inhibited within the depletion region, leading to a longer luminescence lifetime, and a high proportion of erbium ions in the depletion region can be pumped. However, studies of the spatial distribution of optically active erbium ions in the depletion region have demonstrated that there is a dark region within which erbium ions cannot be excited [25]. In fact, only erbium ions near the top of the depletion region can be excited, although in this region the fraction of excited ions can reach 80%.

Note that the processes involved in obtaining carrier-mediated photoluminescence from erbium-doped crystalline silicon are the same as those outlined above with the exception of process I: direct injection of carriers. However, the same problems of Auger de-excitation and backtransfer apply equally to photoluminescence. The first demonstration of erbium photoluminescence in crystalline silicon was published in 1983 by Ennen et al. [27]. The same group followed this 2 years later with the first report of electroluminescence from the same system [28]. Luminescence in both cases was only demonstrated at low temperatures (15 K), and the first demonstration of room temperature photoluminescence from erbium-doped crystalline silicon was not published until 1991 [29]. This was achieved by codoping with oxygen in order to provide a solvation shell around the erbium ion: a key observation was that erbium-doped float-zone single crystal silicon, which has very low concentrations of oxygen, exhibited erbium luminescence intensities two orders of magnitude smaller than Czochralski grown (oxygen-rich) material. Coordination with oxygen is thus a prerequisite for efficient luminescence from erbium-doped silicon, and recent studies of MBE grown material have demonstrated that the Er:O ratio is the most critical factor determining both the optical and electrical properties of the erbium-doped layer [30]. Similar observations apply to codoping with fluorine [31]. Codoping produces electrically and optically active Er–O and Er–F complexes that act as donors in the silicon lattice [32,33]. As well as increasing photoluminescence yield, this has allowed room temperature electroluminescence to be obtained from erbium-doped silicon LEDs [34–36] by greatly reducing the backtransfer process that depopulates the erbium metastable state. The optimum concentration of oxygen for optical activation of erbium in crystalline silicon has been experimentally determined to be around one order of magnitude greater than that of erbium [37]. Note also that the formation of solvation shells around the rare-earth ions through the use of co-dopants considerably increases the solubility of erbium in crystalline silicon.

Studies have shown recently that silicon samples implanted with a thin layer of erbium can exhibit strong erbium photoluminescence when excited from the unimplanted side of the sample (Fig. 8). Given a typical sample thickness of 500  $\mu\text{m}$  and an implantation depth of less than 1  $\mu\text{m}$ , this implies excitation of the  $\text{Er}^{3+}$  centres by carriers diffusing through the bulk material [38]. However,

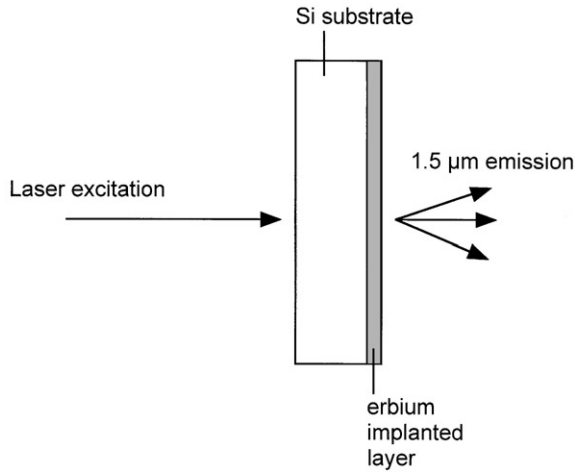


Fig. 8. Schematic of the back-side illumination experiment performed on erbium-doped silicon.

luminescence dynamics studies of this material have shown that the time taken for excitation to reach the erbium layer from the back face is very much longer than would be expected from a consideration of the carrier diffusion rate in bulk silicon. The authors propose that this is a result of the formation of a pn junction by the implanted erbium layer [38]. Excitation cannot flow to the erbium until the junction potential is sufficiently reduced by accumulated charge.

Much work has concentrated on the nature and symmetry of the erbium centre responsible for 1.5  $\mu\text{m}$  emission in silicon, with sometimes contradictory results. Theoretical studies have concluded from energetic considerations that the isolated tetrahedral interstitial erbium site is favoured [39,40]. However, the emitting species in oxygen-doped Er:c-Si has been shown from EXAFS studies to be an Er–O cluster with a six-fold coordination between the central erbium ion and surrounding oxygen ions [41]. The simplest such configuration is an octahedron formed with an erbium atom at the centre and six equally spaced oxygen atoms at the vertices (symmetry  $O_h$ ). However, the crystal field from this arrangement will not provide the required modification of the  $\text{Er}^{3+}$  local environment to make the intra-4f transitions allowed. The active species must therefore be a distorted octahedron. Very recent theoretical work by Ishii and Komukai has investigated different possible configurations of six-fold coordinated by Er–O clusters [42]. Using molecular orbital calculations, the effect of distorting the  $\text{ErO}_6$  octahedron by selectively shortening one, two, or three Er–O bonds to produce species with symmetries of  $C_{4v}$ ,  $C_{2v}$  and  $C_{3v}$ , respectively, have been investigated. It was found that the preferred site has a  $C_{4v}$  symmetry, corresponding to an octahedron in which one Er–O bond has been reduced in length by around 0.1  $\text{\AA}$ . Fig. 9 illustrates the different site symmetries available to erbium in the  $O_h$ ,  $C_{3v}$  and  $C_{4v}$  configurations of the  $\text{ErO}_6$  complex.

The assignment of emission around 1.5  $\mu\text{m}$  in erbium-doped silicon to the  $\text{Er}^{3+}$   ${}^4I_{13/2} \rightarrow {}^4I_{15/2}$  transition should be performed with caution. Crystalline silicon

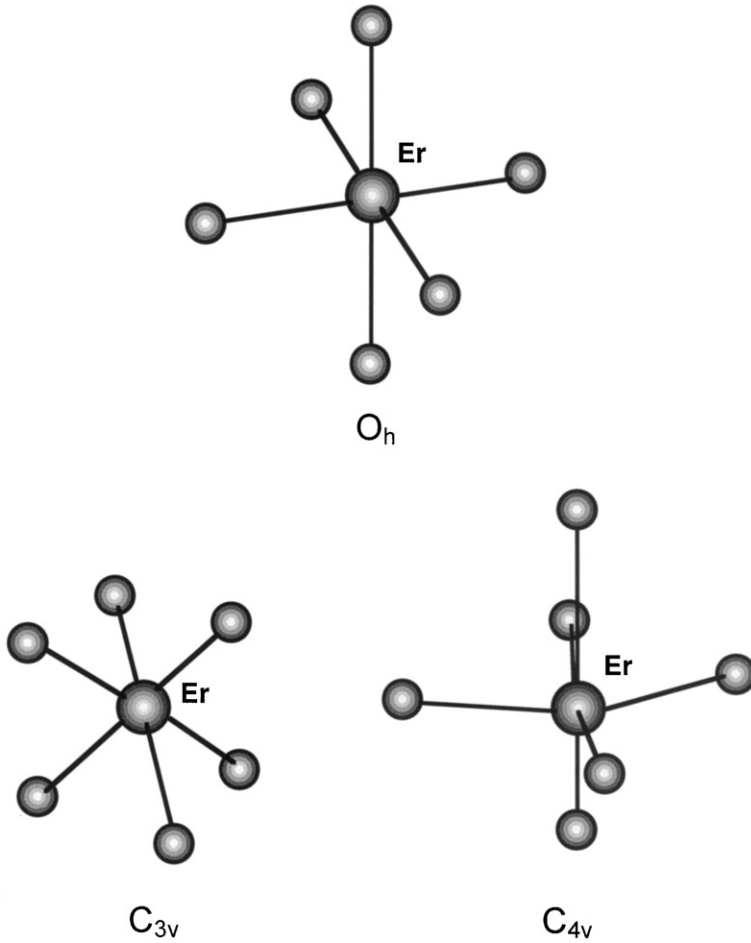


Fig. 9. Different possible point symmetries for the  $\text{ErO}_6$  cluster.

exhibits dislocation luminescence due to the D1 dislocation around  $1.52\ \mu\text{m}$ , which overlaps the erbium transition, and in some cases can appear to have the same lineshape. After high temperature plastic deformation, Si samples exhibit very strong photo- and electroluminescence in the range of the D1 line, which can be detected even at room temperature [43]. Additionally, implantation-related damage can form D1 dislocation loops. In the case of Er-implanted silicon, this can lead to difficulty in assigning the source of emission at  $1.5\ \mu\text{m}$ . Sobolev et al. [44] have studied Er-implanted single crystal Czochralski silicon and have observed emission due to D1 and D2 dislocations ( $1.52$  and  $1.41\ \mu\text{m}$ , respectively) and  $\text{Er}^{3+}$  ions ( $1.53\ \mu\text{m}$ ). Key to the assignment of emission bands is the observation that the D1 emission wavelength shows a dependence on temperature, shifting to longer wavelengths with increasing temperature. Thanks to 4f shielding, the position of the  $\text{Er}^{3+}\ 4\text{I}_{13/2} \rightarrow 4\text{I}_{15/2}$  transition

is insensitive to temperature, though its intensity quenches rapidly above 130 K due to the backtransfer mechanism discussed above.

### 3.1.2. Amorphous silicon

Amorphous silicon is an interesting host for erbium thanks to the increased solubility of Er in a-Si and the ease of codoping with other impurities to activate the 1.54  $\mu\text{m}$  luminescence band. The first report of luminescence from Er-doped a-Si was in 1990 [45], though this material suffers from poor electrical characteristics and defect-mediated luminescence pathways [46], limiting electroluminescence to low temperatures (77 K). However, the use of hydrogenated a-Si overcomes many of these problems [47,48]. The influence of hydrogenation has been widely studied [49], and there have now been a number of reports of electroluminescence from erbium-doped hydrogenated amorphous silicon [50].

Work by Polman et al. on the relative solubility of erbium in crystalline and amorphous silicon has demonstrated that crystallisation of amorphous Er-implanted silicon causes a segregation of the erbium into the amorphous silicon [19]. Single crystal silicon was implanted with a sufficiently high fluence of erbium to amorphise the top 150 Å or so of the substrate. By recrystallising the silicon, the erbium was forced to migrate from the crystalline phase to the amorphous layer and follow the moving phase boundary.

Co-doping amorphous silicon with oxygen greatly improves the luminescence efficiency of the erbium in an analogous way to the bulk silicon case by coordinating the erbium ion with surrounding oxygen ions. Investigations of the local environment of the optically active erbium ions in oxygen-doped hydrogenated amorphous silicon have demonstrated that the luminescent ions are found within Er–O quantum dots [51]. The most likely configuration of these centres is generally thought to be six-fold tetrahedral coordination of the erbium ion with surrounding oxygen ions in  $C_{3v}$  symmetry [67] (Fig. 9). However, bear in mind that the  $C_{4v}$  site suggested by Ishii et al. is also likely [42]. The size of these dots has been estimated to be around that of the unit cell of  $\text{Er}_2\text{O}_3$  (1.05 nm). Evidence for this comes from emission Mössbauer spectroscopy, which demonstrates that the optimal ratio of erbium to oxygen in hydrogenated amorphous silicon is around 10:1, a similar result to that achieved for crystalline silicon.

Recent work has demonstrated that electrical excitation of erbium ions in amorphous silicon proceeds via an Auger process [52]. Injected electrons are captured at a neutral dangling bond  $D_0$  defect located close to an erbium ion. Transfer of excitation to the  $\text{Er}^{3+}$  ion then occurs due to Coulombic interaction.

### 3.1.3. Porous silicon

Since the first demonstration of light emission from electrochemically etched silicon by Canham in 1990 [53], porous silicon has attracted much attention as a material for silicon-based optoelectronics. Confinement of carriers within the nanometer-scale silicon pillars formed by the etching process greatly increases the efficiency of photo- and electroluminescence from silicon, and efficient electroluminescent devices have been made that emit in the visible region [54,55]. A number

of groups have incorporated erbium into porous silicon to produce a 1.5  $\mu\text{m}$  source based on silicon and exploiting the efficient excitation pathways that exist in this material. Doping can be achieved by ion implantation, thermal diffusion, or by electrochemical methods.

The bandgap of the porous silicon host may be readily controlled by varying the etch conditions and therefore the porosity of the material. This may make it possible to activate luminescence from rare earths with luminescence energies greater than the bandgap of bulk silicon. Quantum confinement effects also produce long carrier lifetimes and a high degree of localisation in real space. This may both suppress the Auger backtransfer processes that limit luminescence efficiency in bulk silicon, and increase the interaction probability between the confined carriers and the luminescent rare-earth ions.

Room temperature luminescence has been demonstrated from erbium-doped porous silicon [55–57] in which the optically active erbium is incorporated into the pores of the host by diffusion. After anodic etching to produce porous silicon, the substrate is immersed in a solution of  $\text{ErCl}_3$  and alcohol. Erbium diffuses into the silicon pores, and a subsequent annealing in an oxygen-rich ambient at 1000°C activates the  $\text{Er}^{3+}$  1.5  $\mu\text{m}$  luminescence band. However, the fragile nature of the host can make activation of erbium in porous silicon problematic, as the use of very high annealing temperatures can damage the porous silicon matrix. Recent work has looked at the possibility of capping the porous silicon surface with a layer of silicon nitride to reduce the detrimental effect of high temperatures on the host [58].

The photoluminescence intensity of erbium in porous silicon increases with activation temperature, reaching a maximum around 1100°C. However, the conductivity of porous silicon falls exponentially with annealing temperature [59]. Likewise, increasing both the thickness and porosity (and therefore the degree of quantum confinement) reduces the conductivity. Care must therefore be taken in designing electroluminescent devices from erbium-doped porous silicon. An activation temperature of around 800°C represents a compromise between luminescence efficiency and conductivity, and produces the most intense emission [59].

Electroluminescence studies of erbium-doped porous silicon demonstrate different temperature quenching effects in forward and reverse bias, with very different activation energies. This implies different luminescence mechanisms for the two biasing conditions, which in turn implies at least two erbium-related trap levels in porous silicon. Power efficiencies are low for Er:por-Si electroluminescent devices (0.01%), but are at least comparable to those obtained for devices produced using bulk silicon [59].

Temperature quenching of erbium emission in porous silicon is less pronounced than in crystalline silicon, possibly due to the increased bandgap and the lack of an extended lattice, though luminescence bandwidths are small, at around 10 nm. The luminescence lifetime of the 1.5  $\mu\text{m}$  emission band is around 1.0 ms at room temperature and depends on temperature [60]. Such temperature behaviour suggests that thermal quenching is a result of thermalisation of carriers localised at erbium-related trap levels.

Recent work by Wang et al. has characterised the optical efficiency of different erbium sites in porous silicon [61]. Comparing samples doped by immersion with those implanted with erbium, temperature quenching was much stronger in the latter, implying that the preferred site for efficient luminescence from erbium in porous silicon is at the surface of the pores rather than deeper in the bulk material. This may be due to the influence of oxide layers around the porous silicon nanowires.

Some limited studies have been performed of porous silicon doped with other rare-earth ions, including ytterbium. The luminescent properties of Yb:por-Si are similar to those of Er:por-Si; annealing is required to activate the rare-earth luminescence, and this is dependent on the annealing atmosphere [62]. However, in the case of ytterbium, it appears that activation of the luminescence is best achieved using an oxygen-free annealing atmosphere. This is in contrast to erbium, in which case oxygen readily enhances Er<sup>3+</sup> photoluminescence.

#### 3.1.4. Nanocrystalline silicon

Fully confined semiconductor systems with dimensions less than the excitonic Bohr radius ( $\sim 5$  nm for silicon) exhibit interesting electronic and optical properties thanks to confinement of electrons in one, two or three dimensions depending on the geometry of the structure. Confinement can be produced by amorphous/crystalline, silicon/silica or silicon/air boundaries (for the case of silicon nanopowders [63,64]). Doping these confined systems with rare-earth ions can help to overcome some of the non-radiative de-excitation problems associated with bulk silicon [65]. Key findings of work on these materials are that temperature quenching effects are much reduced and, in common with bulk silicon, 1.5  $\mu\text{m}$  luminescence intensity increases with the oxygen content of the samples [66]. For the case of erbium-doped silicon nanocrystals in an amorphous silicon matrix, photoluminescence data suggest that the optically active erbium ions are located within the amorphous silicon matrix. Excitation is via the absorption bands of the nanocrystals, which transfer excitation to erbium ions in the amorphous matrix [66]. Further evidence from studies of Stark splitting showing eight sharp lines in the emission spectrum of erbium in amorphous/nanocrystalline silicon films suggests that the optically active species is an octahedrally coordinated erbium ion in an ErO<sub>6</sub> complex [67].

There have been a small number of reports of luminescence from erbium incorporated into nanocrystalline silicon in which the confinement is produced by the crystalline–amorphous boundary, including the formation of an erbium-doped ridge waveguide formed from nanocrystalline silicon [68]. Stimulated emission with a threshold of 10 MW cm<sup>-2</sup> was achieved.

#### 3.1.5. Silicon resonating structures

One technique for increasing the luminescence yield of erbium-doped silicon has been to produce resonating structures such as Fabry–Perot microcavities that incorporate the active layer. This has been successfully achieved for amorphous [69] and porous silicon [70,71]. Confinement effects produced by resonating structures produce short luminescent lifetimes, allowing high modulation rates for sources

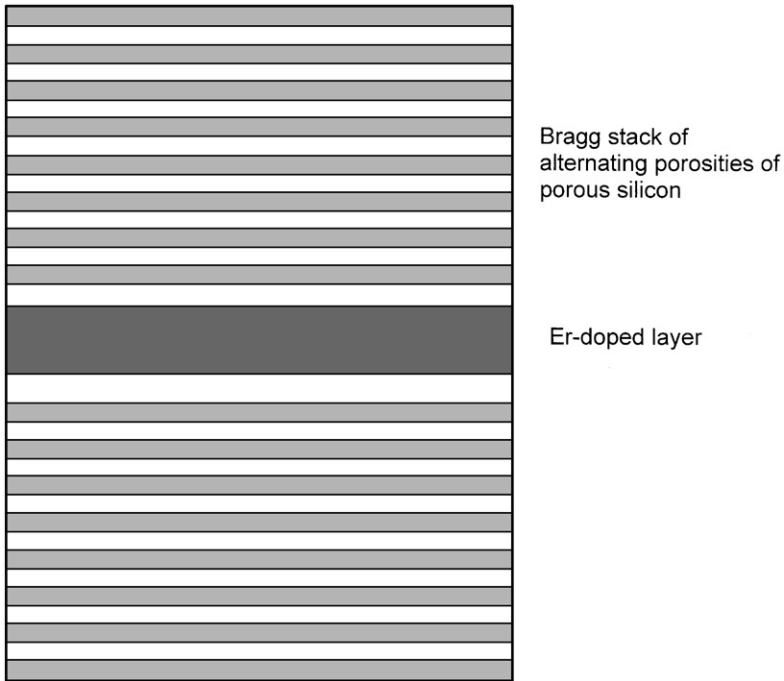


Fig. 10. Schematic of erbium-doped silicon layer surrounded by a Bragg stack of porous silicon of varying porosity, forming a resonant cavity.

based on erbium-doped silicon active layers. The earliest report of enhancing erbium emission in a resonant cavity produced by silicon/silicon dioxide superlattices was that due to Schubert et al. in 1992 [72]. In this case, the structures were produced by rf-magnetron sputtering.

One approach has been to fabricate structures of alternating layers of silicon and silica forming Bragg reflector stacks surrounding a quarter-wavelength thick active erbium-doped layer (Fig. 10), which may be erbium-doped silicon or erbium oxide [73]. Strong confinement produced by high-Q cavities can modify both the spectral linewidth and luminescence lifetime of the erbium emission as well as enhance emission intensity and directivity [74]. Careful design of the microcavity can result in nearly 100% reflectivity in the stop band with a reflectivity minimum at the erbium emission wavelength of  $1.54\ \mu\text{m}$  (Fig. 11).

In the case of porous silicon, multilayer structures can be fabricated by modulating the etching current during sample production. In this way, layers of alternating refractive index may be produced such that Bragg mirrors may be formed on either side of a chosen active layer [75]. Erbium can be introduced into the porous layers using electrochemical doping in which the porous material is immersed in a suitable solution of erbium salt (for example,  $\text{Er}(\text{NO}_3)_3$ -ethanol solution) and a field applied to diffuse the erbium into the porous silicon. Erbium luminescence may be

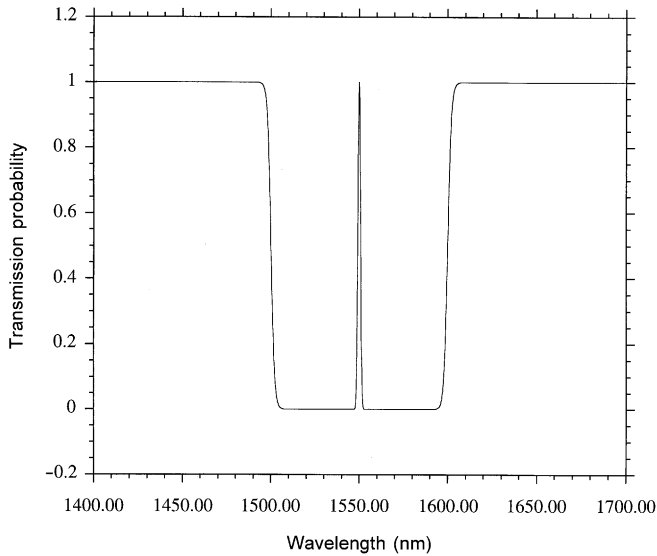


Fig. 11. Ideal transmission characteristics of the structure shown in Fig. 10.

activated by annealing in oxygen, or annealing in a nitrogen atmosphere may optically activate the erbium ions without fully oxidising the porous silicon layers [75]. Such a system produces enhancement and linewidth narrowing of erbium emission, though suffers from the drawback that emission from erbium incorporated in porous layers outside the active region (i.e. within the Bragg mirrors) cannot be suppressed. Care must be taken in the design of the microcavity, as the oxidation/annealing step changes the density, and therefore the refractive index of the porous layers. This results in a wavelength shift in the reflectivity spectrum of the cavity, which must be allowed for in order that the reflectivity minimum overlaps the erbium emission band after annealing.

The periodic nature of the Bragg cavity constitutes a photonic bandgap structure, and therefore the erbium emission from within the cavity is both highly directional and enhanced. Emission through the Bragg stack can be up to 38 times more intense than that in-plane from the side of the sample and is concentrated into a  $20^\circ$  cone around the surface normal [75]. The ability to tailor the cavity structure enables the emission peak to be centred in a wavelength region within which erbium emits only weakly. The luminescence enhancement produced by the cavity therefore compensates for the low yield at these wavelengths.

### 3.1.6. SiGe

Doping silicon with germanium increases its refractive index, and therefore there is interest in forming waveguides in bulk silicon by germanium doping to form buried waveguide structures. Incorporation of erbium into these structures allows the formation of active waveguides, and therefore optical amplifiers in silicon. SiGe also

offers the possibility of changing the band gap of the host by varying the stoichiometry of the alloy, and therefore controlling the host-to-rare-earth excitation exchange mechanism.

Erbium may be incorporated into SiGe layers by either ion implantation or in situ during MBE growth. There have been reports of both photo- [76] and electroluminescence [77] at  $1.54\ \mu\text{m}$  from Er:Si<sub>1-x</sub>Ge<sub>x</sub> samples. The mechanism for excitation of erbium in SiGe is similar to that in silicon, and temperature quenching of luminescence due to Auger backtransfer processes remains a problem. The addition of germanium to silicon causes a reduction in the bandgap energy that is dependent on the germanium fraction, and along with this the erbium luminescence intensity reduces for germanium contents of more than 5 at% [78]. However, the addition of germanium to silicon does not appreciably alter the crystal field surrounding the erbium ions, and therefore the erbium emission spectra in the two materials are nearly identical.

Studies of Si/Si<sub>1-x</sub>Ge<sub>x</sub> multilayer systems have demonstrated an enhancement of low temperature erbium luminescence when erbium is placed in the Si<sub>1-x</sub>Ge<sub>x</sub> layers, compared to placing it in the Si layers. This has been attributed to trapping of photogenerated carriers within the germanium-rich layers [78].

Recent work has demonstrated that strained Si<sub>1-x</sub>Ge<sub>x</sub> layers reduce the occurrence of dislocations in the host material, and as a result erbium luminescence yield is improved and the effects of temperature quenching mitigated [79].

Planar waveguide devices have been produced by forming SiGe waveguides on n-type silicon substrates [80]. Overlaying the waveguide with erbium and carbon co-doped silicon allows electroluminescence from the erbium to be coupled into the SiGe waveguide, and hence edge-emitting devices constructed. The function of the carbon co-dopant was to enhance the erbium emission. Under reverse bias, such devices exhibited  $1.53\ \mu\text{m}$  electroluminescence (FWHM in the region of 30 nm) at room temperature, though temperature quenching meant that the intensity was reduced by a factor of  $\sim 7$  from that observed at 105 K.

### 3.2. Gallium arsenide and other III–V hosts

The first reports of rare-earth 4f luminescence in III–V hosts were in the early 1980s [81,82]. GaAs, InP, GaP, AlGaAs, and GaInP have all been investigated as hosts for rare-earth ions, though luminescence yield is low and temperature quenching effects are strong. Nonetheless, rare-earth doped III–V hosts offer the potential for integration of rare-earth luminescence with semiconductor microelectronics, though more recent work has concentrated on rare-earth doped silicon.

Erbium-doped gallium arsenide has been the subject of study for some time, and in fact GaAs was the first erbium-doped semiconductor to exhibit photoluminescence at  $1.5\ \mu\text{m}$  in 1982 [82]. Further reports of incorporation of optically active erbium into GaAs by MBE and liquid phase epitaxy (LPE) were made in 1987 [83,84]. Erbium is thought to exist in substitutional sites in GaAs, replacing Ga ions. Er-related emission from GaAs is rather weak compared to other semiconductors, and temperature quenching produces a reduction of PL intensity of a factor of 5 or more

on heating samples to room temperature. However, the incorporation of nitrogen into amorphous Er:GaAs films can both increase luminescence intensity (by a factor of up to 50) and decrease temperature quenching effects [85]. There is a correlation between nitrogen content and bandgap for GaAs:N. Thus pure GaAs has a bandgap around 1.55 eV, whilst incorporating 40 at% nitrogen into GaAs:N results in an increase of this to around 2.6 eV. The increase in luminescence efficiency is therefore postulated to be a result of the increase in excitonic ionisation energy. Increasing the nitrogen content further results in modification of the host to produce GaN. Thus, GaAs:N can be considered as a halfway house between GaAs and GaN. However, there are problems associated with increasing the nitrogen content of GaAs, including phase separation of GaN and GaAs.

Care needs to be taken when producing erbium-doped gallium arsenide to avoid carbon contamination: Er:C complexes formed in the semiconductor host are not electrically active, and therefore quench electroluminescence.

Oxygen co-doping of Er:GaAs both enhances the 1.5  $\mu\text{m}$  emission and changes the shape of the spectrum, producing a smaller number of sharp lines. This is likely to be due to the formation of Er–O complexes similar to those seen in silicon. Although there are a number of different erbium sites in Er:GaAs:O, PLE measurements have suggested that the optically active Er centre is an Er atom substituted for a Ga atom coupled to two oxygen atoms substituted on nearby arsenic sites [86]. This is supported by Zeeman measurements that have suggested the site has a  $C_{2v}$  symmetry [87].

Excitation of rare-earth luminescence in GaAs is via the recombination of bound excitons at rare-earth trap states. For the cases of ytterbium and erbium, these states lie at 0.65 and 0.67 eV from the conduction band edge, respectively (in the case of oxygen-codoped Er:GaAs, the trap level is estimated to be 0.42 eV [86]). Studies have shown that the exciton binding energy in Yb:GaAs (0.77 eV) is too low to produce emission from  $\text{Yb}^{3+}$ , which accounts for the absence of luminescence from this system [88]. A strong Auger backtransfer mechanism similar to that seen in erbium-doped crystalline silicon results in temperature quenching of luminescence.

Although erbium can in principle be incorporated into gallium arsenide at rather high concentrations (Peaker et al. [89] reported no evidence of a limit to Er incorporation by MBE at levels up to  $2 \times 10^{20} \text{ cm}^{-3}$ ), the solubility of optically active erbium in gallium arsenide by equilibrium growth processes is rather low, at  $7 \times 10^{17} \text{ cm}^{-3}$ . Above this limit, ErAs precipitates are formed, quenching the 1535 nm emission [90]. At high concentrations, such precipitates can also be formed during MBE growth. They form a self-organising set of spherical quantum dots with the rocksalt structure, in contrast to the zinc blende structure of the surrounding gallium arsenide [89]. By changing the substrate temperature during MBE growth, the average diameter of the precipitates can be varied between 1 and 2.2 nm. Precipitate formation and growth proceeds at the sample surface by surface migration of erbium rather than by Ostwald ripening [91]. By varying the gallium and arsenic flux during growth, complex dendritic ErAs structures can be produced which have been termed “quantum trees” [92]. Similar self-organising effects have been reported for thulium-doped gallium arsenide [93].

Growth of gallium arsenide at low temperatures (200–300°C) results in material with a slight excess of arsenic (~1 at%) and a high concentration of gallium vacancy sites. Such material (LT-GaAs) is highly resistive and exhibits very short photo-carrier lifetimes (sub-nanosecond). Despite the high concentration of defects, erbium-implanted LT-GaAs exhibits 1.54  $\mu\text{m}$  emission following annealing at 650°C [94].

Indium phosphide has received some considerable attention as a host for rare-earth ions, particularly ytterbium, as this is a convenient system for studying excitation transfer between the semiconductor host and the rare-earth ion. Ytterbium substitutes for indium on lattice sites, principally due to the similar sizes of the In and Yb ions. The ytterbium luminescence spectrum in InP is insensitive to the sample production technique, in contrast to other III–V systems, and also the energy levels of  $\text{Yb}^{3+}$  are simple (Fig. 3), resulting in only one type of luminescence centre being formed in a range of hosts. It has been found in this system that excitation of the rare-earth ion occurs by a process similar to that found in other semiconductors: the Yb is promoted to its excited state by the recombination of an electron–hole pair at a Yb trap state in the band gap [95]. Auger backtransfer provides a strong temperature-quenching effect in a similar way to that seen in Er-doped silicon and gallium arsenide [96].

Electroluminescent devices have been produced from erbium-doped GaAs, erbium-doped GaP [97], and neodymium-doped GaAs [98].

### 3.3. Wide bandgap semiconductors

Bandgaps larger than 2 eV (i.e. covering those materials whose bandgap energies fall firmly within the visible or near-UV range) are, somewhat arbitrarily, classed as wide. Technologically important materials in this category include gallium nitride, silicon carbide, silicon nitride, aluminium nitride, zinc sulphide, zinc oxide, and diamond. Semiconductor nitrides are specifically of interest thanks to their compatibility with existing semiconductor technologies, and gallium nitride in particular has received much attention [99]. The temperature-quenching effects that plague rare-earth ions in silicon and other semiconductors are found to be inversely proportional to the bandgap of the host [100], making wide bandgap materials attractive choices for rare-earth incorporation. For electrical activation of rare-earth emission, as in carrier-mediated luminescence mechanisms such as that observed in Er:Si and Er-doped III–V hosts, the efficiency of excitation is thought to depend on the ionisation energy of excitons bound to  $\text{Er}^{3+}$  centres. Wide bandgap materials have higher excitonic ionisation energies, and therefore are more efficient hosts for electrically activated rare-earth emission.

In contrast to silicon, research on rare-earth doped wide bandgap materials has covered both visible and infrared emission from the rare-earth ions.

#### 3.3.1. Gallium nitride

Rare-earth doping of gallium nitride is still a very new area, and as yet there are only a small number of groups active in the field: principally those of Steckl, Bishop,

Zavada, and Abernathy of the universities of Cincinnati, Urbana-Champaign, and Florida, Gainesville. However, progress has been rapid, particularly in the area of erbium-doped gallium nitride [101]. A recent review was published by Steckl and Zavada [102], though the rapid development of this area makes it difficult to provide an authoritative and up-to-date account. The following is therefore a snapshot of the current status of the field.

Gallium nitride possesses a number of properties that make it a suitable host for visible- and infrared-emitting rare-earth ions, including a wide and direct bandgap, good chemical and thermal stability, excellent high field transport properties, and ready incorporation of rare-earth ions at relatively high concentrations. In common with other group III nitrides, GaN also exhibits a remarkable insensitivity to the presence of relatively high concentrations of defects, enabling emission to be obtained from materials containing densities of defects that would effectively quench emission in smaller bandgap materials. In fact, it now appears that defects can often play an important role in activating rare-earth emission, and the engineering of defect centres to produce tailored activation channels and emission bands is an important new area of research (see below). This is particularly fortuitous in view of the difficulty in growing defect-free gallium nitride.

Generally, gallium nitride is grown on either silicon or sapphire substrates by MBE using solid, gaseous or metal-organic sources. The most common crystal structure produced by these methods is hexagonal, in which the Ga atoms occupy sites of  $C_{3v}$  symmetry. Rare-earth ions are either grown during deposition, or subsequently implanted, and studies have indicated that the preferred rare-earth site is a relaxed substitutional gallium site [103], although the rare-earth ions can form aggregates at high temperature in a similar fashion to that seen in other hosts. The solubility of rare-earth ions in gallium nitride is very much higher than in silicon and other narrow gap semiconductors: optically active erbium concentrations of up to  $2 \times 10^{21}$  ions/cm<sup>3</sup> have been reported in GaN grown on silicon [104]. Erbium can be incorporated into gallium nitride in at least four different chemical environments, all of which have been shown to be optically active at 1.5  $\mu\text{m}$  [101,121].

The first report of visible emission from erbium in gallium nitride was that due to Steckl and Birkhahn in 1998 [105]. MBE-grown erbium-doped GaN films were prepared on sapphire substrates and were found to exhibit intense green emission around 540 and 560 nm due to the  $\text{Er}^{3+} \ ^2\text{H}_{11/2} \rightarrow \ ^4\text{I}_{15/2}$  and  $\ ^4\text{S}_{3/2} \rightarrow \ ^4\text{I}_{15/2}$  transitions. Emission in these bands is either due to the above-bandgap pumping of the GaN host and a consequent excitation transfer to the rare-earth ion, or can result from upconversion processes involving the absorption of combinations of 840 nm and 1  $\mu\text{m}$  photons by  $\text{Er}^{3+}$ . Fig. 12 shows an energy level diagram of  $\text{Er}^{3+}$  with the upconversion steps marked corresponding to the absorption of (a) two 840 nm photons, (b) one 840 nm photon and one 1  $\mu\text{m}$  photon. Both processes excite electron from the  $\ ^4\text{I}_{15/2}$  ground state to higher energy level manifolds ( $\ ^2\text{H}_{9/2}$ ,  $\ ^4\text{F}_{3/2}$ , or  $\ ^4\text{F}_{7/2}$ ), from which non-radiative relaxation to either the  $\ ^2\text{H}_{11/2}$  or  $\ ^4\text{S}_{3/2}$  levels results in radiative relaxation to the ground state and consequent emission at 523 and 546 nm, respectively [106]. More recent work has demonstrated visible emission in gallium

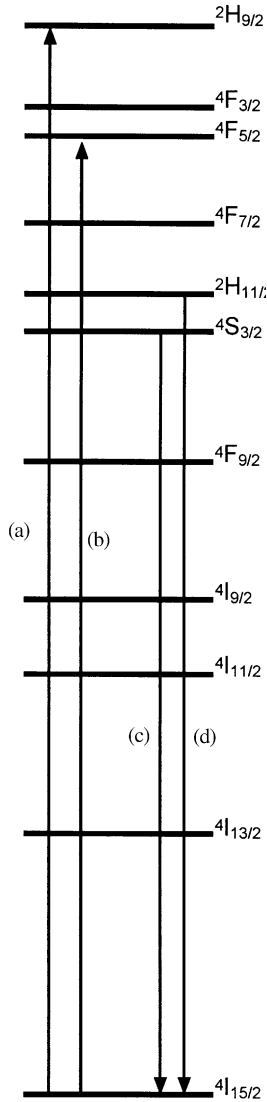


Fig. 12. Multiphoton absorption steps of visible emission from erbium in gallium nitride.

nitride from higher-lying  $4f$  levels of a number of other rare-earth ions, including praseodymium [107], europium [108], dysprosium [109], and thulium [110]. Both photoluminescence and electroluminescence have been demonstrated, and mixed colour emission from material doped with more than one rare earth has been reported [102].

The role of defects in rare-earth doped gallium nitride is an interesting one in that they act as centres through which carrier-mediated excitation of the luminescent

rare-earth ions can proceed. Broad absorption features at energies below the GaN bandgap, due to the presence of defects or impurities, couple to the rare-earth ions and provide an efficient indirect excitation mechanism. This is in addition to direct excitation via rare-earth absorption bands and indirect excitation from above-bandgap absorption of the GaN host [118]. However, defects, particularly those caused by ion implantation of rare earths into GaN, can also provide effective non-radiative loss mechanisms, principally by either acting as charge-trapping centres that reduce the population of carriers available for excitation of the rare-earth ions, or by inducing an optical absorption band around 1540 nm [111]. Thus, samples prepared using ion implantation must be annealed to remove implantation damage, typically at temperatures in excess of 1000°C [112], though, as in silicon and silica, annealing at too high a temperature reduces rare-earth luminescence due to clustering. In addition, high temperature annealing can change the composition and structure of the GaN matrix. Luminescence studies of the sites occupied by erbium in implanted GaN have suggested the existence of a range of different local environments for the rare-earth ions [113,114]. In particular, a comparison of visible luminescence spectra from above-gap and resonant excitation indicated that the single exponential decay from resonantly pumped erbium becomes non-exponential when pumped above-gap. Narrower emission linewidths and the presence of fine structure in the emission spectra for resonant excitation suggested that in this case only a subset of the available erbium ions is excited. High temperature annealing can lead to structural rearrangement that preferentially activates different configurations. Luminescence studies of the  $\text{Er}^{3+} \ ^4\text{I}_{13/2} \rightarrow \ ^4\text{I}_{15/2}$  band have in fact suggested the presence of nine separate erbium emission centres, each produced by a different interaction with impurity, defect, or complex centres in the GaN matrix [115]. Each of the nine centres can be selectively excited through the appropriate choice of pump wavelength corresponding to one of the below-gap absorption bands associated with the particular defect or impurity. Non-radiative transfer to the optically active erbium results in intra-4f emission around 1.5  $\mu\text{m}$ . However, the majority of active erbium ions (>99%) appear to be associated with only one of the nine centres, as only one of the emission lines can be excited by direct intra-4f absorption. This centre has been identified as an isolated  $\text{Er}^{3+}$  ion substituted on a Ga site [116]. Moreover, it is not possible to excite this centre with a comparable efficiency using above-bandgap excitation. This suggests that those erbium ions participating in the indirect non-radiative excitation processes represent less than 1% of the total available population of rare-earth ions [115]. This opens up the possibility of modifying the efficiency of the erbium–impurity interaction by codoping with appropriate ions to increase the capture cross-section of the impurity centres and thereby increasing the efficiency of above bandgap optical or electrical excitation of the rare-earth ion. Studies using magnesium as a codopant in Er:GaN have in fact demonstrated enhancement of one of the impurity–erbium coupling channels, characterised by a broad absorption band in the 2.8–3.4 eV region [115]. The reasons for this enhancement are not yet clear: it is possible that the Mg dopant ion is directly incorporated into the trap centre responsible for the absorption band, or alternatively, Mg has a catalytic effect on trap formation. Much work remains to

be done, but indications are that the optical and electrical properties of Er:GaN may be tailored by the appropriate choice of codopant.

In contrast to erbium-doped silicon, non-radiative recombination processes in erbium-doped gallium nitride are thought to be weak, and the quantum efficiencies of green emission from the erbium  $^4S_{3/2} \rightarrow ^4I_{15/2}$  and  $^2H_{11/2} \rightarrow ^4I_{15/2}$  transitions have been estimated to be close to unity [114].

The infrared transitions of the rare-earth ions have not been totally neglected in gallium nitride work: the first observation of strong 1.5  $\mu\text{m}$  emission from  $\text{Er}^{3+}$ -doped and oxygen co-doped GaN was made in 1994 [117]. Recent work by Thaik et al. has demonstrated extremely weak thermal quenching of infrared emission from erbium and oxygen co-implanted gallium nitride films [118]. Significantly, a reduction of only around 10% of the integrated PL intensity of the 1.5  $\mu\text{m}$  band is seen on increasing the sample temperature from 15 to 550 K. This transition, of course, remains of key interest for telecommunications applications, and LEDs functioning at 1.5  $\mu\text{m}$  have been fabricated from erbium-doped gallium nitride [119].

Photoluminescence excitation studies of the 1.5  $\mu\text{m}$  band in erbium-doped gallium nitride have enabled the measurement of the absorption cross-sections of the second and third excited states ( $^4I_{11/2}$  and  $^4I_{9/2}$ , respectively) [120]. Surprisingly, and in contrast to erbium-doped glasses, that for the  $^4I_{9/2}$  level was larger than that of the  $^4I_{11/2}$  state ( $1.65 \times 10^{-20}$  and  $4.8 \times 10^{-21} \text{ cm}^2$ , respectively). The reason for this remains unclear. The same group reported a higher room temperature PL intensity at 1.5  $\mu\text{m}$  compared to that at 77 K, a very surprising result.

Work has been performed on the excitation mechanism of 1.5  $\mu\text{m}$  emission produced by above bandgap pumping of Er:GaN. Kim et al. demonstrated that the photoluminescence spectrum produced using 325 nm excitation is the sum of spectra obtained by pumping at 632.8 and 458 nm [121]. The conclusion drawn from this was that  $\text{Er}^{3+}$  luminescence from above gap excitation results from a trap-mediated mechanism rather than direct optical pumping to a high level erbium-excited state.

Codoping erbium-doped GaN with impurity elements such as oxygen or carbon increases the intensity of 1.5  $\mu\text{m}$  emission, as well as decreasing temperature quenching effects [122]. The formation of Er–C and Er–O complexes produces the required wavefunction mixing to make the intra-4f transitions partially allowed. Moreover, the implantation of oxygen to a concentration one order of magnitude greater than that of the rare-earth ion does not change the substitutional site of the erbium ions [103]. Recent work comparing oxygen- and carbon-codoped Er:GaN has concluded that oxygen is the better codopant, producing much weaker temperature quenching even for relatively low oxygen concentrations ( $< 10^{19} \text{ cm}^{-3}$ ) [123]. Additionally, carbon impurities in GaN sit mid-gap, resulting in a high resistivity material. This is in contrast to oxygen, which acts as a shallow donor. However, technological considerations mean that for reasons of chamber contamination it is undesirable to introduce oxygen into MBE chambers during GaN growth. Studies have shown that an Er:O concentration ratio of at least 1:5 is necessary for saturation of photoluminescence from the 1.5  $\mu\text{m}$   $\text{Er}^{3+}$  band. However, incorporation of too high a concentration of oxygen can quench this

luminescence band, perhaps due to the incorporation of oxygen into the nitride matrix [101].

### 3.3.2. Silicon carbide

Silicon carbide exhibits the same temperature insensitivity as does gallium nitride. Studies on erbium-implanted SiC have demonstrated intense  $1.5\ \mu\text{m}$  emission in a number of different SiC polytypes, all of which show a relatively weak temperature quenching effect [124]. The luminescence intensity from erbium-doped silicon carbide is nearly constant for temperatures between 2 and 400 K. Room temperature electroluminescence has been demonstrated in erbium-implanted SiC pn junction under forward bias, though the quantum efficiency was very low ( $7.5 \times 10^{-6}$ ) [125].

## 4. Rare-earth ions in insulators

Rare-earth luminescence was first reported in glasses and crystals, and rare earths (particularly erbium) in waveguide materials remain the most important and thoroughly researched application of rare-earth ions for optoelectronics. An excellent and thorough review of research on erbium-doped glasses for optical amplification was published by Miniscalco in 1991 [15]. Since then there has been progress on novel glasses including fluorides, tellurites, and glasses containing silicon nanoclusters. Fibre amplifiers are now a relatively mature and widely deployed technology, offering large gains, low noise figures, and broad bandwidths. However, there is still a drive to increase gain bandwidths and also to develop active planar waveguides.

### 4.1. Silica

From the perspective of optoelectronics, silica is of interest as a host for rare-earth ions primarily because of its deployment in fibre technology and the importance of the  $\text{Er}^{3+}$   $1.5\ \mu\text{m}$  emission band in telecommunications applications. For this reason, much of the work in this field has centred on optimising erbium solubility and in emission in silica-based glasses for fibres and planar waveguides.

Rare-earth solubility in silica is limited to relatively modest concentrations by clustering and ion–ion interactions. The trivalent rare-earth ions occupy octahedrally coordinated sites in silica with six nearest neighbour oxygen atoms. Typical Er–O bond lengths are in the range  $2.25\text{--}2.3\ \text{\AA}$  [19]. It appears that the formation of stable  $\text{ErO}_6$  species is a prerequisite for efficient luminescence in silica (recall that this is also true of silicon: codoping with oxygen activates erbium luminescence through the formation of  $\text{ErO}_6$  clusters).

The development of silica-based optical fibres in the 1970s heralded a revolution in telecommunications and promised vastly increased bandwidths by exploiting optical rather than electrical transmission. Progress since the early days of fibre technology has resulted in fibres with extremely low losses at telecommunications wavelengths, and figures of  $0.2\ \text{dB km}^{-1}$  at  $1550\ \text{nm}$ , close to the theoretical limit of  $0.1\ \text{dB km}^{-1}$ ,

are now typical. However, even at these loss levels, signal degradation over very long spans remains a problem requiring some form of amplification. Exploiting the intra- $4f$   $^4I_{13/2} \rightarrow ^4I_{15/2}$  transition of the  $\text{Er}^{3+}$  ion has enabled the development of all-optical amplification in the ultra-low-loss window of silica optical fibre and it is this technology that dominates research into luminescence from rare-earth doped silica. Although the principal application of this material has been in fibre technology, there is a significant interest in planar waveguides for use in optical integrated circuits. Such integration is driven by the increasing interest in such applications as WDM, optical computing, planar lasers, and nanotechnology. However, concentration quenching effects have limited the amount of optically active rare earth that can be included in the silica matrix, and therefore long active regions have been required for erbium-doped amplifiers. Although not an insurmountable problem for fibre-based amplifiers, in which long lengths of lightly doped fibre can be employed, this poses a challenge to the development of planar waveguide amplifiers.

The tendency to exhibit concentration quenching varies considerably with glass composition. Thus, for example, soda-lime silicate glass is capable of accommodating up to 2 at% erbium without precipitation, while pure silica has an upper limit of around 0.1%. The degree of clustering (and hence ion-ion interaction) also depends upon the thermal history of the glass. Melt glasses show a much higher tendency to form rare-earth precipitates, whilst implanted or low temperature chemical vapour deposition (CVD) (e.g. plasma-enhanced chemical vapour deposition (PECVD)) samples can accommodate higher concentrations of unclustered rare-earth ions. This is due to the reduced diffusion of dopant ions in the matrix.

In contrast to erbium-doped silicon, in which short luminescent lifetimes are required in order to produce directly modulated sources capable of very high modulation rates, the emphasis in erbium-doped silica is on long luminescent lifetimes to enable efficient population inversion, and hence optical amplification.

#### 4.1.1. Fibres

The outstanding success story of rare-earth doped materials over the past decade or so has undoubtedly been the optical amplifier based on erbium-doped aluminosilicate fibre. The advent of the EDFA has enabled much of the recent progress in long-haul telecommunications, and has helped to standardise the 1.5  $\mu\text{m}$  band as the communications band of choice. The EDFA is now becoming a mature technology, and commercial amplifiers now have very low noise figures, linear gain responses and, thanks to gain equalisation techniques, relatively flat gain profiles. The following section is a very brief discussion of some of the issues that are the most pressing in the search to produce wider bandwidth, more efficient amplifiers. For a more comprehensive discussion of currently deployed EDFA technology, the reader is directed elsewhere [12,126].

Erbium is readily incorporated into silica, albeit at relatively low concentrations due to clustering effects, and, whilst the erbium absorption and emission cross-sections are small in silica (typically in the range  $10^{-20}$ – $10^{-21}$   $\text{cm}^2$ ), the non-radiative backtransfer losses that plague silicon are largely absent. As a result, luminescence lifetimes are long (up to 12 ms). The relatively low solubility of erbium in silica is

largely due to its tendency to cluster to form aggregates that can be of the order of tens of nanometers in diameter or larger. Interaction between erbium ions within clusters, and coupling between adjacent clusters, leads to rapid non-radiative decay of the  $\text{Er}^{3+} \ ^4\text{I}_{13/2}$  metastable level. This severely limits both the photoluminescence intensity achievable from erbium-doped silica, and the lifetime of the  $\ ^4\text{I}_{13/2}$  metastable state. Long lengths of lightly doped fibre are therefore required in order to achieve sufficient gain. In addition, the erbium emission band in silica is very narrow (11 nm), and for practical applications the silica matrix is modified by the addition of a small quantity of alumina to the mix. This increases the bandwidth of the emission to around 45 nm and also improves the solubility of erbium to allow higher concentrations of optically active ions to be included [126]. The optimum concentration of aluminium ions is around twice that of the rare earth, though care must be taken, as aluminium microclusters form at aluminium concentrations higher than 14 at%.

Although emission can be readily obtained across the 1530–1560 nm range, gain can be very non-uniform across this band. The inhomogeneously broadened emission spectrum of erbium in silica has a strong peak at around 1535 nm with a shoulder at 1550 nm, and therefore some method for either flattening the gain spectrum or compensating for its non-uniformity is desirable. As a result, there is considerable effort directed at flattening the gain profile by filtering, by devising new pumping schemes, and by altering the host material. The simplest method is to run the amplifier at 70% inversion, in which case, although the overall gain is somewhat reduced from the 100% inversion case, the gain spectrum is flat between 1530 and 1560 nm [126]. This is the most commonly used technique, but with the requirement for gain outside these wavelengths, higher inversion factors must be used, in which case other solutions must be found, including gain flattening filters and varying the pump wavelength and power at different points in the fibre amplifier. However, such solutions are complicated and costly, and as a result there is a drive to find new hosts with broad and flat gain spectra.

The 1528–1560 nm gain band is now referred to as the *C*-band (*conventional* band), but is not the only wavelength region under investigation. The long wavelength region (*L*-band) from 1570 to 1600 nm and the short wavelength *S*-band are both the subject of much research. In the long wavelength region, in particular, devices now exist that exhibit flat gain profiles and reasonable gain coefficients [127,128]. However, the *L*-band gain is very dependent on pump wavelength, and there is much work directed at alternative pumping schemes [129], including pumping at 1530 nm, within the *C*-band gain spectrum [128]. Optimisation of the fibres can increase the gain in the *L*-band and significantly reduce the lengths of fibre required. Broad-band amplification may then be obtained by integrating *L*- and *C*-band amplifiers, by using Raman/*C*-band hybrid amplifiers, or by changing the host material to one that exhibits a much wider gain spectrum (for example, tellurites).

Work has been carried out on reducing the tendency of rare earths to form clusters in solid hosts. Broadly speaking, this has taken two approaches: production of erbium-doped materials (principally silica) by non-thermal low-temperature techniques such as PECVD [130], and dispersion of clusters formed in thermally

grown material by post-processing [131]. The latter technique employs a fast pulse from an excimer laser to deliver sufficient thermal energy to a rare-earth cluster to break it up: if the pulse is short enough, the rare-earth ions are effectively “frozen” in their new positions and the concentration of unclustered rare-earth ion thereby increased. Such experiments have demonstrated a 95-fold increase in luminescence from europium-implanted sapphire and an 85-fold increase in luminescence from europium-implanted silica on laser processing [131].

#### 4.1.2. Waveguides

Considerable work has been done on the production of the planar analogue of the EDFA. Integration of optics onto planar substrates is a very attractive technology and there are a number of groups working on the production of planar gain elements using erbium-doped waveguides. Such devices may be readily integrated with other optical elements such as splitters and multiplexers/demultiplexers all on one substrate. Because of this and their small size, they are very attractive for application in local area networks and the next generation of WDM technology.

Production of such devices can be either by ion implantation or low-temperature growth techniques such as PECVD or sputtering followed by photolithography to produce ridge waveguides.

A major limitation in work on active planar devices has been the solubility limit of erbium in silica. Although not as severe as the low solubility of erbium in silicon, erbium begins to precipitate in melt glasses at concentrations around 0.1 at%, resulting in luminescence quenching and thus requiring very long active regions for appreciable gain. Such aggregates can in fact reach macroscopic size and act as scattering centres. This can potentially preclude the production of compact waveguide devices. However, the use of low temperature deposition techniques such as PECVD can raise the solubility limit by around an order of magnitude, thereby allowing the production of much smaller devices [130]. Ion exchange and sol-gel glasses have been investigated as materials for waveguide fabrication, along with sputtering, laser ablation, and direct writing using focused ion beams or lasers.

A considerable amount of research has been directed at ion implantation of silica glasses and overcoming the problems associated with implantation related damage, ion-ion interaction, and activation of the erbium ions [19]. Even directly after implantation, erbium-implanted silica exhibits strong 1.5  $\mu\text{m}$  emission. However, on annealing in an inert atmosphere (nitrogen or argon), the luminescence intensity can be increased by a factor of four or more up to a peak annealing temperature around 950°C. Beyond this point, thermally induced diffusion of erbium ions results in aggregation and quenching. Lifetime quenching in implanted samples is strongly dependent on implantation damage even for very low fluences ( $10^{11}$  ions  $\text{cm}^{-2}$  and greater), and is proportional to the mass of the implanted ion [19]. A, perhaps unintended, bonus of this sensitivity is that erbium ions can be used as a probe for irradiation damage in a variety of applications [1]. However, for the purposes of telecommunications, care must be taken to eliminate such defects.

Germanosilicate glasses are of particular interest for waveguides, as for fibres, because of their photosensitivity. This allows the production of refractive index

gratings by directly periodically modifying the refractive index of the glass using high-power UV lasers in a similar way to the production of fibre gratings [132]. Recent work has demonstrated the production of erbium-doped  $\text{SiO}_2\text{-GeO}_2\text{-Al}_2\text{O}_3$  waveguides using sol-gel techniques [133].

Polman and co-workers have studied the effect of implantation damage on the tendency of erbium ions to cluster in soda-lime glass films [134]. Samples were implanted with a low fluence of erbium ions and then subsequently implanted with a series of increasing fluxes of gold ions to induce increasing degrees of structural damage to the host. Very little change to the lifetime of the  $^4\text{I}_{13/2}$  level was observed, in contrast to very strong lifetime quenching in samples in which the secondary implants were of erbium ions, thereby inducing  $\text{Er}^{3+}$  clustering. In contrast to this, luminescence lifetimes in borosilicate glasses implanted with similar concentrations of erbium ions were around four times shorter for Er densities above  $2 \times 10^{20} \text{ cm}^{-3}$ . It is likely that the presence of boron in the glass matrix enhances the implantation-related damage.

#### 4.2. Silicon-rich silica

A material that has been attracting attention recently as a host for luminescent rare-earth ions is silicon-rich silica. This material consists of silica doped with excess silicon in the form of nanometer-sized clusters or crystallites. It can be thought of as a three-dimensionally confined silicon system in which the confinement is produced by the silicon-silica boundary, and is therefore in some respects analogous to the nanocrystalline silicon hosts discussed previously. The embedded silicon clusters may be either amorphous or crystalline, and because of quantum confinement effects, emit light in the visible and near-infrared region. Such material has been studied for some time as a promising candidate for light emission from silicon [135–137]. Photoluminescence efficiencies are low [138], as it is generally thought that even for nanoclusters as small as 2 nm in diameter, the silicon remains predominantly indirect gap. However, when co-doped with rare-earth ions the situation is dramatically improved: intense rare-earth emission can be obtained, and doping with erbium allows access to the 1.5  $\mu\text{m}$  spectral region.

Indirect excitation of erbium photoluminescence via coupling between the absorption bands of the silicon nanoclusters and erbium excited states has been demonstrated by a number of groups [139–142]. Fig. 13 shows the photoluminescence excitation spectrum of a sample of silicon-rich silica containing 10 at% excess silicon in the form of nanoclusters, and 0.5 at% erbium. Also shown is an absorption spectrum of erbium-doped stoichiometric silica in the same region, indicating the position of erbium absorption bands. This figure clearly illustrates that the presence of silicon nanoclusters enables the excitation of erbium ions at wavelengths away from erbium absorption bands. Quantum confinement effects can be used to tailor the absorption band edge of the silicon nanoclusters and move it into the visible region [137]. Absorption of incident photons then proceeds via the broad-band absorption of the nanoclusters, producing confined excitons. This step is followed by rapid excitation exchange to the rare-earth ions and consequent luminescence at

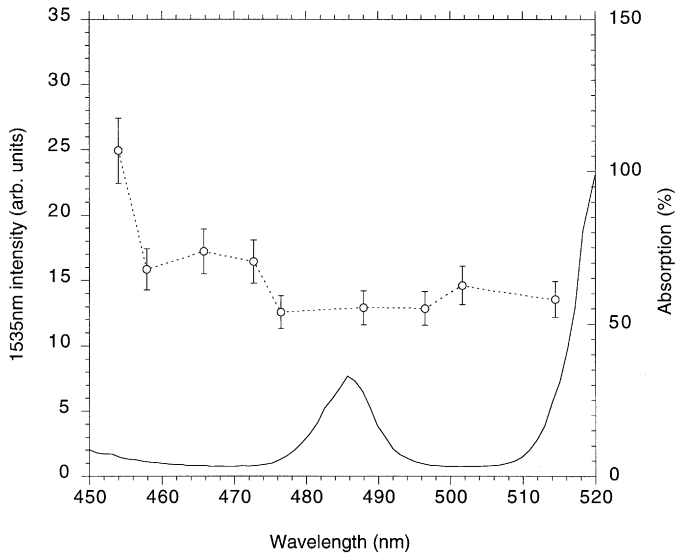


Fig. 13. Photoluminescence excitation spectrum of erbium-doped silicon-rich silica (· · · ·). Also shown is an absorption spectrum of a stoichiometric silica fibre doped with erbium (—).

1.5  $\mu\text{m}$  from the erbium metastable state. Luminescence from the silicon nanoclusters is in competition to that from the rare-earth ion, though by using a sufficiently high rare-earth concentration silicon nanocluster luminescence can be effectively quenched. It is likely that the transfer takes place via a dipole–dipole interaction leading to population of (as yet unspecified) higher excited states of the erbium ion that feed into the  $^4I_{13/2}$  metastable state via rapid photon-assisted decay. A rate equation analysis of this process is described in work published by groups in Catania [142] and University College London [143,144], and proceeds as follows:

Firstly, the population of excitons in the nanoclusters is given by

$$\frac{dN_{\text{ex}}}{dt} = \sigma\phi(kN - N_{\text{ex}}) - \frac{N_{\text{ex}}}{t},$$

where the number of excitons ( $N_{\text{ex}}$ ) is proportional to the pump flux ( $\phi$ ), the absorption cross-section ( $\sigma$ ), the concentration of nanocrystals ( $N$ ), and is limited by a factor  $k$  which governs the maximum number of excitons that can exist in a single cluster. The second term represents recombination of excitons within the nanocluster.

Next, the population of the erbium metastable state is described by

$$\frac{dN_{\text{Er}}^*}{dt} = (1 - C)R^* + C\sigma_{\text{Er}}\phi - \frac{N_{\text{Er}}^*}{\tau_{\text{Er}}},$$

where  $N_{\text{Er}}^*$  is the concentration of the excited rare-earth ions,  $R^*$  is the increase of the excited rare-earth population through energy transfer from an exciton to the

appropriate excited state;  $C$  is the proportion of excitation of  $\text{Er}^{3+}$  attributed to direct absorption of pump photons ( $0 \leq C \leq 1$ ),  $\sigma_{\text{Er}}$  is the direct optical absorption cross-section of  $\text{Er}^{3+}$ , and  $\tau_{\text{Er}}$  is the decay lifetime for the  $\text{Er}^{3+}$  metastable state, taking into account both radiative and non-radiative processes. Here,

$$R^* = \frac{N_{\text{ex}}(\eta N_{\text{Er}} - N_{\text{Er}}^*)A}{\tau_{\text{tr}}},$$

where  $A$  is an interaction volume within which excitation exchange takes place (related to the parameter  $R_0$  in Förster–Dexter theory),  $\tau_{\text{tr}}$  is the interaction time, and  $\eta$  is a quantum efficiency term which takes into account two factors: firstly that the efficiency of the transfer from excitons to rare-earth ions will not be 100%, and secondly that only a fraction of the excited  $\text{Er}^{3+}$  will decay to the appropriate metastable level of  $\text{Er}^{3+}$  and hence increase the metastable state erbium population. This equation also allows for upconversion: i.e. the process whereby an erbium ion in the metastable state is excited to higher energy states by transfer from excitons, and therefore does not contribute to the emission process.

Making the assumption that the population of excitons reaches a steady-state well before that of  $\text{Er}^{3+}$ , the solution of the above equations is

$$N_{\text{RE}}^* = A \left[ 1 - \exp \left( - \left( \frac{(1 - C_{\text{Dir}})N\Lambda}{\tau_{\text{tr}}} \frac{\sigma\tau\phi k}{\sigma\tau\phi + 1} + C_{\text{Dir}}\sigma_{\text{Er}}\phi + \frac{1}{\tau_{\text{d}}^{\text{RE}}} \right) t \right) \right],$$

where

$$A = \frac{(1 - C_{\text{Dir}}) \frac{N_{\text{RE}}\eta N\Lambda}{\tau_{\text{tr}}} \frac{\sigma\tau\phi k}{(\sigma\tau\phi + 1)} + C_{\text{Dir}}\sigma_{\text{Er}}\phi N_{\text{RE}}}{(1 - C_{\text{Dir}}) \frac{N\Lambda}{\tau_{\text{tr}}} \frac{\sigma\tau\phi k}{(\sigma\tau\phi + 1)} + C_{\text{Dir}}\sigma_{\text{Er}}\phi + \frac{1}{\tau_{\text{d}}^{\text{RE}}}}.$$

This allows an effective cross-section for indirect excitation of the erbium metastable state to be defined as

$$\sigma_{\text{eff}} = \frac{\sigma\tau k N\Lambda}{\tau_{\text{tr}}}.$$

Measurements of 1.5  $\mu\text{m}$  luminescence intensity and rise time as a function of pump photon flux enable two independent measurements of this cross-section to be made. Work by groups in Catania [142] and University College London [143] performed on material produced by both ion implantation and PECVD has shown that the presence of silicon nanoclusters can increase the effective absorption cross-section of erbium in silica by four orders of magnitude to around  $7.33 \times 10^{-17} \text{ cm}^2$ . Fig. 14 shows reciprocal luminescence rise-time data as a function of photon flux for a sample of erbium-doped silicon-rich silica, along with a fit to this data using the above model.

Because the initial absorption of pump photons is by the broad-band absorbing silicon nanoclusters, the constraints on pump wavelength are considerably relaxed. Instead of requiring a narrow-band pump source tuned to one of the  $\text{Er}^{3+}$

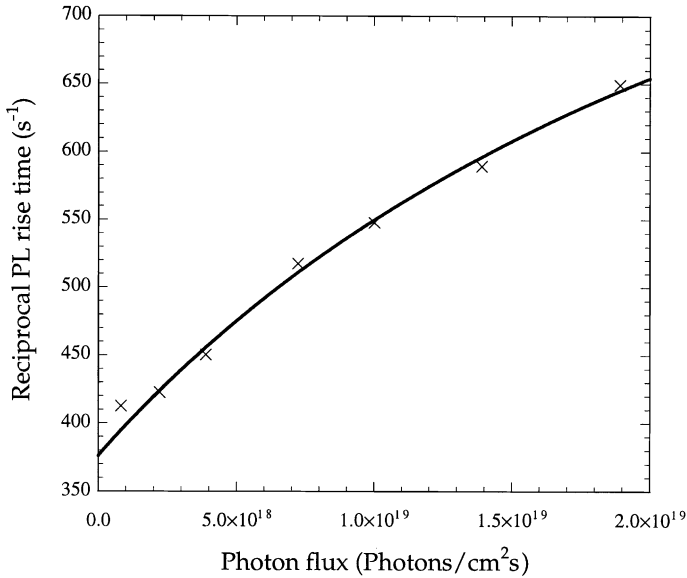


Fig. 14. Reciprocal luminescence rise times for 1.53  $\mu\text{m}$  luminescence as a function of 476 nm pump photon flux for erbium-doped silicon-rich silica.

absorption bands, broad-band sources can be used. The University College London group have demonstrated pumping of  $\text{Er}^{3+}$  emission in silicon-rich silica using a commercial camera flashgun [145]. This opens up the possibility of cheap flashlamp-pumped erbium-doped optoelectronic components. Recent work has demonstrated optical gain at 1.53  $\mu\text{m}$  of  $4 \text{ dB cm}^{-1}$  in a ridge waveguide structure of silica doped with silicon nanocluster [146]. Excitons were generated in the silicon nanoclusters using the 476 nm line from an argon-ion laser: by using this wavelength, excitation of the erbium ions was predominantly by excitation exchange from the silicon nanoclusters. Excitation levels were in the region of  $1.5 \text{ W cm}^{-2}$ . This is an extremely significant result, as it opens up the possibility of broad-band pumped erbium-doped gain elements and possibly a silicon-based laser.

Very recently, electroluminescence has been achieved from an erbium-doped silicon-rich silica [147] and silicon nanolayer/silica films [148]. In the case of the former, thin layers of erbium-doped  $\text{SiO}_x$  were deposited by magnetron sputtering onto silicon substrates. Ohmic contacts were diffused into the bottom of the substrate and gold contacts evaporated onto the top surface of the samples. Electroluminescence results showed lower threshold and increased efficiency over a similarly produced erbium-doped silicon device. In the case of the silicon nanolayer samples, a thin layer of silicon ( $d < 4.0 \text{ nm}$ ) was deposited by magnetron sputtering onto a film of erbium-doped silica grown on a silicon substrate (both n+ and p were used) and a top contact of gold used for electrical connection. The thin silicon layer constituted a confined system from which excitation could be transferred to the erbium ions in the silica layer in an analogous way to that seen in erbium-doped

SiO<sub>x</sub>. The intensity of the electroluminescence was found to be strongly dependent on the thickness of the nanometre-scale silicon layer.

Similar electroluminescence studies have been performed on the rare-earth doped silica layers incorporated into MOS devices [149]. Both erbium and terbium have been employed as the optically active rare-earth ion and have been implanted into 50 nm SiO<sub>2</sub> layers. Erbium ions are excited by hot electrons as a result of Fowler–Nordheim tunnelling, which produces electrons with average energies in excess of 5 eV. In the case of the erbium-doped device, an enhancement of  $\sim 7$  times was seen in the EL from the MOS structure when compared to that from an erbium-doped pn diode. Internal efficiencies of  $> 4 \times 10^{-5}$  and impact excitation cross-section of  $1 \times 10^{-15} \text{ cm}^2$  were reported.

Some work has been performed on silicon-rich silica doped with a range of rare-earth ions other than erbium, including Pr, Tm and Eu [142]. Similar excitation exchange mechanisms were found to operate in each case.

### 4.3. Alumina

Recently, aluminium oxide (Al<sub>2</sub>O<sub>3</sub>) has been studied both as a host for rare-earth ions, in particular erbium, and as a material for waveguide fabrication [19]. Principal reasons for this are the high solubility of erbium in alumina and the high refractive index of the matrix ( $n = 1.64$ ), which make it possible to produce silica-clad fibres and waveguides that exhibit high optical mode confinement and are capable of small bend radii. The increased solubility of Er in Al<sub>2</sub>O<sub>3</sub> over that in SiO<sub>2</sub> results from the valence match between the rare-earth dopant ( $3^+$ ) and the substituted cation (Al<sup>3+</sup>). The optically active Er<sup>3+</sup> ion readily substitutes for aluminium ions occupying octahedral sites in alumina. Moreover, in the Al<sub>2</sub>O<sub>3</sub> lattice one-third of Al<sup>3+</sup> octahedral sites are unoccupied, and hence a large number of Er<sup>3+</sup> ions can be incorporated without suffering from pair-induced upconversion [150]. In addition, the Er<sup>3+</sup> emission linewidth can extend to up to 55 nm in alumina [152], compared to around 11 nm in pure silica, making erbium-doped alumina waveguides promising candidates for WDM applications.

Recently, production of Er-implanted [151] and Er-doped Al<sub>2</sub>O<sub>3</sub> thin films by PECVD has been reported [152]. A net optical gain of 2.3 dB has also been reported from a 4-cm long erbium-implanted Al<sub>2</sub>O<sub>3</sub> optical waveguide pumped at 1.48  $\mu\text{m}$  with 9 mW of launched optical power [153].

Despite its potential usefulness, one drawback of the Er system is its lack of absorption bands corresponding to the emission wavelength of low cost pump sources. To help overcome this, Yb-sensitisation is used to alleviate constraints on the pump wavelengths. Yb exhibits an intense and broad absorption band between 800 and 1080 nm, spanning several convenient pump wavelength source options. Recently, Er/Yb co-implanted alumina thin films have been produced and the indirect excitation of Er<sup>3+</sup> through energy exchange from Yb has been studied [154]. In addition, Yb sensitisation of the Er system has been demonstrated to improve amplification in short erbium-doped waveguide amplifiers in which high erbium concentrations cause pair-induced upconversion [155]. Although erbium in alumina

does not suffer from pair-induced upconversion [150], the uniform upconversion process between two excited Er ions is still present (i.e., one Er ion is promoted to the upper level while the second ion decays to the ground level), reducing pump efficiency and thus signal gain.

Very recently, Chryssou et al. investigated signal gain in short Yb-sensitised erbium-doped alumina waveguide amplifiers [156]. A rate equation analysis was employed that assumed pumping at a wavelength of 980 nm and two competing  $\text{Er}^{3+}$  excitation mechanisms: absorption by ytterbium ions followed by excitation transfer to optically active erbium ions, and direct optical absorption by  $\text{Er}^{3+}$  ions. In addition, excited state absorption at 980 nm from the  $\text{Er}^{3+} {}^4\text{I}_{11/2}$  metastable level to the  ${}^4\text{F}_{7/2}$  level was taken into account. This work showed that co-doping with ytterbium reduces the detrimental effect of uniform upconversion. Signal gains as high as 13 dB are predicted in 5 cm long optical waveguides.

#### 4.4. Lithium niobate

Lithium niobate has received attention as a host for rare-earth ions because of the possibility of exploiting its electro-optic, acousto-optic and nonlinear properties to produce a range of rare-earth doped integrated optoelectronic devices from modulators to switches and filters [157,158]. Doping can be achieved readily by thermal diffusion, ion exchange [159], or by ion implantation [160]. Most work on this material has concentrated on erbium doping to produce devices for the 1.5  $\mu\text{m}$  telecommunications window, and a number of erbium-doped  $\text{LiNbO}_3$  waveguide devices, including lasers and planar amplifiers, have been produced [161,162]. Such devices have so far been produced by thermal diffusion of erbium into lithium niobate. However, being an equilibrium process, rare-earth clustering limits the maximum concentration of optically active erbium that can be incorporated into the host. For this reason, much attention has recently been paid to implantation doping of lithium niobate [163].

The lattice site of the erbium ions in the host is critical to the optical properties of the material [164], and it is generally thought that  $\text{Er}^{3+}$  ions occupy distorted  $\text{Li}^+$  substitutional sites with  $\text{C}_3$  point symmetry [165]. Evidence for this comes from X-ray, ESR and luminescence studies, and two such sites are thought to exist, characterised by different displacements of the erbium ion around the  $\text{Li}^+$  site. Very detailed spectroscopic studies of the  ${}^4\text{F}_{9/2}$  to  ${}^4\text{I}_{15/2}$   $\text{Er}^{3+}$  transition by Gill et al. [166] have suggested the existence of six erbium sites distinguished by degrees of ion clustering. More recently, however, Mignotte has suggested the existence of a niobium substitutional site [167] in materials prepared by ion implantation.

Following implantation, thermal activation of erbium luminescence is required by annealing at temperatures around 500°C. However, the amorphisation produced by the implantation process is not removed until the sample is recrystallised at 1060°C [167]. At such temperatures, some diffusion and clustering of the rare-earth ions occur, necessitating an annealing procedure that is a compromise between optical activation of the erbium ions and crystallinity of the lithium niobate matrix. Nevertheless, the technique is promising for the production of planar devices.

Co-operative upconversion in  $\text{LiNbO}_3$  is much less of a problem than is the case for Er-doped silica ( $C_{\text{up}} < 1.4 \times 10^{-19}$  cf.  $3 \times 10^{-18} \text{ cm}^3 \text{ s}^{-1}$  for stoichiometric silica). This is attributed to the narrower absorption and emission spectra of erbium in lithium niobate, a consequence of which is the reduced probability of resonant energy transfer processes [19].

Recent work has looked at visible emission from erbium-doped lithium niobate waveguides for application as tunable visible or near-IR lasers.

#### 4.5. Low phonon hosts

Hosts with low phonon energies reduce the probability of multiphonon non-radiative decay from rare-earth excited states, and therefore allow near- and mid-infrared transitions that are not seen in hosts such as silica (phonon cut-off energies around  $1100 \text{ cm}^{-1}$ ). However, many of the physical and chemical properties of these materials that are responsible for the low phonon energies also make the materials delicate and susceptible to chemical attack. This can be mitigated through careful choice of glass composition, and also by the use of appropriate coatings and protective layers.

Low phonon hosts are also required to enable efficient emission from  $\text{Tm}^{3+}$ , which is not possible in silica. Thulium is a very attractive rare-earth dopant that can potentially provide gain between 1400 and 1520 nm using readily available and cheap laser pump sources around 790 and 1064 nm. The advent of very low –OH content fibres makes amplification close to 1400 nm a possibility, and it may also be possible to use gain-shifted thulium-doped materials at wavelengths around 1600 nm. However, power conversion efficiencies are low for thulium-doped amplifiers (typically around 2%) as a result of the small branching ratio of the Tm 1460 nm transition. Problems with coupling to silica phonons mean that Tm is likely to be deployed in low phonon hosts rather than silica or alumina.

Fig. 15 shows an energy-level diagram for  $\text{Tm}^{3+}$ , demonstrating that it is a four-level system, in contrast to the three-level  $\text{Er}^{3+}$  system. Pumping at 790 nm populates the  $^3\text{H}_4$  metastable state from which de-excitation is possible via two radiative pathways involving the emission of 800 or 1460 nm photons, with branching ratios of 90% and 8%, respectively. Additionally, photoluminescence efficiency is extremely dependent on host: low phonon energies are required for high efficiency, which limit the choice of host to fluoride glasses, tellurites, and multicomponent Sb-silicate glasses.

Although the branching ratio,  $\beta$ , is small for the Tm 1460 nm emission band, the short luminescence lifetime of the  $\text{Tm}^{3+}$  ion in tellurite hosts is due to a high emission probability rather than competitive non-radiative de-excitation through multiphonon decay. Thus, the quantum efficiency of emission at 1460 nm ( $\eta$ ) can be of the order of 90%, and the product  $\beta\eta$  is greater in thulium than in praseodymium. However, there remains a persistent problem of a competing emission process at 800 nm. Tanabe and co-workers have adopted a number of co-doping schemes to reduce this [168], including using a combination of  $\text{Ho}^{3+}$  to quench the  $\text{Tm}^{3+}$  first excited state and  $\text{Eu}^{3+}$  to quench the resultant  $\text{Ho}^{3+}$  to  $\text{Tm}^{3+}$  backtransfer.

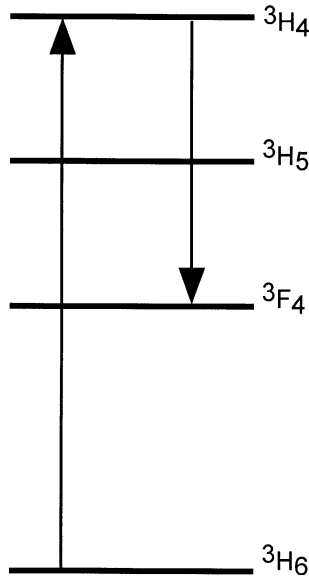


Fig. 15. Energy levels of  $\text{Tm}^{3+}$ : absorption of a 790 nm photon accesses the  $^3\text{H}_4$  state, from which 1460 nm emission results from the transition to the  $^3\text{F}_4$  state. Note that the branching ratio for this transition is only 8%.

However, a more promising scheme proves to be the use of  $\text{Nd}^{3+}$ -doped cladding around a  $\text{Tm}$ -doped tellurite fibre. The neodymium radiatively quenches the 800 nm  $\text{Tm}^{3+}$  transition (which overlaps the  $\text{Nd}^{3+}$  absorption at 800 nm), and as it is in the cladding rather than the fibre, it does not quench the  $\text{Tm}^{3+}$  1460 nm emission band (this quenching being a non-radiative process).

#### 4.5.1. Fluorides

Fluoride glasses have photon energies around half of those of silica, with vibrational cut-off energies around  $550\text{ cm}^{-1}$ , (Table 2), and therefore give access to a range of optical transitions not accessible in other hosts. For telecommunications applications, fluorides are attractive because of their very low minimum intrinsic losses. Quoted values for the theoretical minimum are in the region of  $0.02\text{ dB km}^{-1}$  at  $2.5\text{ }\mu\text{m}$  for ZBLAN compared to  $0.15\text{ dB km}^{-1}$  at  $1.55\text{ }\mu\text{m}$  for silica. However, this level has yet to be achieved, principally due to processing difficulties, and practical loss levels in such materials are in the region of  $1\text{--}2\text{ dB km}^{-1}$ . A wide range of fluoride and fluorophosphate compositions have been studied with a number of rare-earth dopants in order to optimise rare-earth emission and overcome some of the mechanical and chemical stability problems that can affect fluoride hosts [169]. Fluoride glasses are generally multicomponent in order to maximise their mechanical and chemical stability. The most common formulation for optoelectronic purposes is ZBLAN ( $\text{ZrF}_4\text{--BaF}_2\text{--LaF}_3\text{--AlF}_3\text{--NaF}$ ) and its variants. Praseodymium, neodymium, and thulium all require low-phonon hosts for luminescence at  $1.3$  and  $1.4\text{ }\mu\text{m}$ ,

Table 2  
Maximum phonon energies of different host materials

Host	Maximum phonon energy (cm <sup>-1</sup> )
Silica	1100
Tellurite (75 mol% TeO <sub>2</sub> )	750
Fluoride glass (ZrF <sub>4</sub> )	400–600
ZBLAN	590
Chalcogenide sulphide glass	400–450
Chalcogenide selenide glass (As <sub>2</sub> Se <sub>3</sub> )	220–230

and longer wavelength transitions such as the 2.7  $\mu\text{m}$   ${}^4\text{I}_{11/2} \rightarrow {}^4\text{I}_{13/2}$  emission band of erbium are accessible in these hosts. Rare-earth doped fluoride glasses are also used to produce upconversion fibre lasers [170]. The low phonon cut-off energies mean that the efficiency of the two-photon absorption processes required for upconversion is much higher than in silica. As an example, Tm<sup>3+</sup>-doped ZBLAN fibres have produced > 200 mW of 480 nm light when pumped by three 1150 nm photons [171].

The concentration quenching effects seen in silica are much reduced in fluoride glasses, and as an example, there have been reports of the incorporation of up to 18 mol% of optically active erbium into ZBLAN (although at such high concentrations, the erbium dopant is better regarded as one of the glass components and the composition of the “host” becomes ZrF<sub>4</sub>–BaF<sub>2</sub>–ErF<sub>3</sub>–AlF<sub>3</sub>–NaF). Emission at both 980 nm and 1.5  $\mu\text{m}$  has been observed in such highly doped material [172].

Interest in optical amplification at 1.3  $\mu\text{m}$  (corresponding to the first low-loss window in silica optical fibres) has driven research into Nd<sup>3+</sup>- and Pr<sup>3+</sup>-doped fluoride glasses. Much work has been directed towards producing the praseodymium analogue of the EDFA [173,174] to further extend the capabilities of silica fibre networks. Recently, Nd<sup>3+</sup> has emerged as the leading contender for gain in this spectral region, having a larger stimulated emission cross-section and excited state lifetime than praseodymium. Pump sources at 800 nm, corresponding to the Nd<sup>3+</sup>  ${}^4\text{I}_{9/2} \rightarrow {}^4\text{F}_{5/2}$  transition are readily available, and this band has a large absorption cross-section. In addition, concentrations of 1 mol% or more are achievable without significant quenching. However, the lifetime of the Nd<sup>3+</sup> excited state is much shorter than that of Er<sup>3+</sup> in silica: around 100–500  $\mu\text{s}$  in ZBLAN, resulting in a low quantum efficiency of less than 4% for the 1.3  $\mu\text{m}$   ${}^4\text{F}_{3/2} \rightarrow {}^4\text{I}_{13/2}$  transition [175]. In addition, strong excited state absorption processes lead to absorption around 1.3  $\mu\text{m}$ , precluding gain around this wavelength. ESA occurs from the  ${}^4\text{F}_{3/2}$  level to three higher states:  ${}^2\text{K}_{13/2}$ ,  ${}^4\text{G}_{7/2}$ , and  ${}^4\text{G}_{9/2}$  levels, and the ESA spectrum overlaps the short wavelength portion of the emission spectrum. This limits the gain to wavelengths longer than 1.31  $\mu\text{m}$  in Nd<sup>3+</sup>-doped ZBLAN [176].

The other side of the excited state absorption coin is that fluoride glasses can be efficient hosts for upconversion processes, as mentioned in the context of producing fibre upconversion lasers, and also as has been demonstrated for both Er<sup>3+</sup>- and

$\text{Pr}^{3+}$ -doped aluminium fluorophosphates [177]. In the case of erbium-doped  $\text{AlF}_3\text{--MgF}_2\text{--CaF}_2\text{--SrF}_2\text{--BaF}_2\text{--YF}_3\text{--ZrF}_4\text{--NaPO}_3$ , pumping at 514.5 nm produced up-conversion luminescence around 400 nm from the  $^2\text{P}_{3/2}$  to  $^4\text{F}_{15/2}$  transition. Upconversion is due to both excited state absorption and excitation exchange between neighbouring erbium ions. These processes are favoured by the very low vibrational energies of the fluorophosphate host, which significantly reduce the probability of multiphonon relaxation processes from the higher energy levels of the  $\text{Er}^{3+}$  ion.

Host crystallinity appears to have an influence on emission intensity in fluoride glasses. MacFarlane et al. have investigated erbium-doped fluoride hosts that have been partially crystallised by controlled annealing [178]. The resultant fluoroaluminate glass ( $19\text{BaF}_2\text{--}28\text{AlF}_3\text{--}5\text{CaF}_2\text{--}15\text{MgF}_2\text{--}5\text{NaF--}30\text{ErF}_3$ ) contained a high density of nanocrystals in the size range 8–12 nm diameter. Photoluminescence studies demonstrated enhancement of Er emission at both 1.54  $\mu\text{m}$  and 670 nm, along with linewidth narrowing of the red transition (670 nm). The chemical nature of the crystalline phase(s) is unclear, but the implication of the observed line narrowing is that a proportion of the optically active  $\text{Er}^{3+}$  ions are somehow associated with the nanocrystals. Similarly, luminescence enhancement is likely to be due to the presence of erbium in ordered phases. Similar results have been reported for erbium-doped partially crystallised fluorozirconate glasses [179]. A novel approach has been to employ a mixed glass–ceramic host containing small crystallites, around 10 nm in diameter. Using a mixed fluoride–oxide matrix to overcome some of the durability problems associated with fluoride hosts, a lifetime of up to 3 ms for the  $\text{Er}^{3+}$  2.7  $\mu\text{m}$  emission band was obtained, implying weak phonon coupling [180].

Fluorochlorides are a special class of fluoride glasses that have an increased transmission range in the infrared as well as higher refractive indices. Although chemical stability is degraded in these systems (they are particularly prone to degradation due to exposure to water), their optical properties are very promising. Poulain and co-workers at the University of Rennes have studied praseodymium-doped fluorochlorogallate and fluorochloroindate glasses, in which they have achieved quantum efficiencies of around 7% for the  $^1\text{G}_4 \rightarrow ^3\text{H}_5$  luminescence transition [181]. This is approximately double the value obtained in  $\text{Pr}^{3+}$ -doped ZBLAN. Results from this study also suggested that the local environment around the rare-earth ion is very sensitive to the starting materials used in the production of the host, as well as the presence of impurities with high phonon cut-off energies that act as non-radiative decay channels. However, chemical stability remains a particular problem in these materials, as a result of which they have yet to find practical application.

#### 4.5.2. Chalcogenides

Chalcogenide glasses are those containing the chalcogen elements S, Se, and Te, and can be binary ( $\text{As}_2\text{S}_3$ ,  $\text{As}_2\text{Se}_3$ ) or multicomponent ( $\text{Ge}_{20}\text{S}_{40}\text{Br}_{40}$ ). They are transparent in the infrared up to wavelengths of around 10  $\mu\text{m}$ . Chalcogenide glasses have a number of properties that make them promising hosts for rare-earth ions: as

well as low phonon energies ( $400\text{--}450\text{ cm}^{-1}$  for sulphides and  $350\text{ cm}^{-1}$  for selenides) [182]; they exhibit high refractive indices, no  $\text{--OH}$  absorption band, high photosensitivity (allowing easy fabrication of gratings) and very high optical nonlinearities [183]. Interestingly, they also exhibit a strong coupling between the host matrix absorption and the rare-earth emission bands, allowing broad-band optical pumping of rare-earth luminescence [184]. Both erbium [183,184] and neodymium [185] have been investigated as dopants. The combination of low phonon energies and infrared transparency enables emission to be obtained at much longer wavelengths than would be achievable in other hosts [186]. Thus, emission at  $2.7$ ,  $3.5$ , and  $4.5\text{ }\mu\text{m}$  has been measured from erbium-doped chalcogenides, praseodymium-doped glasses have extended this out to  $4.9$  and  $7.2\text{ }\mu\text{m}$ . There is indirect evidence for emission as far out as  $8.0\text{ }\mu\text{m}$  in Tb-doped chalcogenide fibres [187].

Laser oscillation at  $1.08\text{ }\mu\text{m}$  has been achieved in neodymium-doped chalcogenides and amplification has been demonstrated at  $1.08$  and  $1.34\text{ }\mu\text{m}$  using  $\text{Nd}^{3+}$  and  $\text{Pr}^{3+}$  doping, respectively. Recent work comparing chalcogenide and fluoride hosts for praseodymium-doped fibre amplifiers concentrated on the Ga–Na–S system, chosen for its thermal stability and capability for doping with reasonable levels of rare earth [188]. Although gain was observed in the wavelength range  $1325\text{--}1350\text{ nm}$ , absorption due to the  ${}^3\text{H}_5\text{--}{}^1\text{G}_4$  transition precluded gain at shorter wavelengths. The low phonon energy of this glass meant that the  ${}^3\text{H}_5$  level has a sufficiently long lifetime to maintain a significant population, leading to excited state absorption around  $1310\text{ nm}$ . However, a hybrid fibre device that employed both fluoride and chalcogenide hosts produced a gain spectrum flat to within  $2\text{ dB}$  between  $1290$  and  $1330\text{ nm}$ .

For telecommunications applications, dysprosium exhibits emission around  $1.3\text{ }\mu\text{m}$  in sulphide (GaLaS [189]) and selenide (GeAsGaSe) [182] glasses. The transition is between the 3rd/4th excited states ( ${}^6\text{H}_{9/2}/{}^6\text{F}_{11/2}$ : the two levels are so close in energy that they can be regarded as one band) and the  ${}^6\text{H}_{15/2}$  ground state. Internal quantum efficiencies in the two hosts were  $29\%$  and  $94\%$ , respectively, though multiphonon quenching of the upper  ${}^6\text{H}_{9/2}/{}^6\text{F}_{11/2}$  state is a problem thanks to the small gap ( $1800\text{ cm}^{-1}$ ) between this and the lower lying second excited state ( ${}^6\text{H}_{11/2}$ ).

#### 4.5.3. Tellurites

Multicomponent oxide glasses in which the major component is  $\text{TeO}_2$  are classified as tellurites. Tellurite glasses have a very wide transparency range ( $350\text{ nm}$  to  $5\text{ }\mu\text{m}$ ), relatively low phonon cut-off energies ( $750\text{ cm}^{-1}$ ), and good corrosion resistance and mechanical stability. They have high refractive indices, which in turn can result in increased radiative transition rates for rare-earth ions [190]. Erbium-doped tellurites offer the advantage of increased bandwidth over silica [191,192], and devices with gain-flattened bandwidths of up to  $80\text{ nm}$  have been reported [193,194]. Recently, a hybrid fibre amplifier using a parallel combination of a tellurite EDFA and a  $\text{Tm}^{3+}$ -doped fibre was reported, exhibiting a gain bandwidth of  $113\text{ nm}$  [193]. Tellurite glasses are efficient hosts for upconversion emission from erbium and

ytterbium [195], and have nonlinear refractive indices, which make them suitable for second harmonic generation [196].

A recent comparison of tellurite glasses (75 mol% TeO<sub>2</sub>) with binary fluorides (AlF, ZrF, etc.) as host materials for erbium suggested that both co-operative upconversion and excited state absorption are reduced in the tellurite host [190]. A study by Shibin Jiang's group at the University of Arizona of highly erbium-doped tellurite glasses calculated absorption and emission cross-sections and quantified upconversion coefficients and excited state absorption [197]. In particular, the  $^4I_{13/2} \rightarrow ^4I_{9/2}$  cooperative upconversion coefficients of  $2.74 \times 10^{-18} \text{ cm}^3 \text{ s}^{-1}$  were found to be more than an order of magnitude lower than that in phosphosilicate hosts ( $9.0 \times 10^{-17} \text{ cm}^3 \text{ s}^{-1}$ ) and comparable to that in silica ( $3.0 \times 10^{-18} \text{ cm}^3 \text{ s}^{-1}$ ).

Although tellurite-based devices have yet to be widely deployed, a number of theoretical studies have demonstrated their potential for application in WDM and DWDM systems. Measurements on erbium-doped material have shown that high concentrations of optically active erbium can be incorporated (around 2.5 at%), and emission cross-sections at 1535 nm of up to  $1.3 \times 10^{-20} \text{ cm}^2$  are achievable [197,198]. Erbium-doped tellurite waveguides have been produced by ion exchange [199], which provides good depth control and a uniform concentration profile through the waveguide.

Because of their low phonon cut-off energies, tellurites have been investigated as hosts for thulium for application in optical amplifiers in the 1.4  $\mu\text{m}$  region [168]. Although Tm concentrations must remain low in order to reduce cross-relaxation, Tm:tellurites codoped with holmium show sufficiently high quantum efficiencies to be considered for amplifiers. By adding a cladding layer doped with neodymium, the competitive Tm<sup>3+</sup> emission at 800 nm can be effectively quenched by coupling to the Nd<sup>3+</sup> absorption band.

## 5. Rare-earth ions in polymers and organic hosts

A number of properties make polymers attractive hosts for rare-earth ions, including low cost, ease of fabrication on a wide range of substrates, low dispersion, and broad luminescence bands. A recent review by Sloof et al. of this field summarises recent developments and outlines some of the problems associated with doping organic materials with inorganic rare-earth salts [200]. Despite such concerns, there has been some success in producing optically active rare-earth doped organic materials, and polymers doped with neodymium [201,202], europium [203], and erbium [204] have all been used to produce waveguide optical devices that have exhibited gain.

Recent results on terbium-doped polysiloxane films have shown intense photoluminescence at 545 nm from the  $^5D_4$  to  $^7F_5$  transition, even from as-deposited films [205]. Significantly, the deposition of the polymer film on a porous alumina substrate enhanced the photoluminescence output. This is possibly due to the porous nature of the substrate facilitating the production of carbon dots within the pores

that increase the efficiency of optical pumping of the rare-earth ion in a similar way to silicon nanoclusters in silica.

Inorganic erbium compounds cannot be used as rare-earth sources for producing doped polymers, as they are immiscible with organic solvents. However, encapsulation of erbium ions in organic ligands produces a precursor that can be easily dispersed in polymer films. The properties of a range of such ligands were studied by Sloof et al. [206], who used both cyclic and acyclic polydentate cage complexes to encapsulate optically active erbium ions. All samples exhibited luminescence at  $1.5\ \mu\text{m}$ , though lifetimes were in the sub-microsecond regime due to quenching of the emission by  $-\text{OH}$  groups in the organic solvent. Despite this, calculations showed that polymer waveguides incorporating erbium complexes may exhibit optical amplification with a net gain around  $1.7\ \text{dB cm}^{-1}$ .

Recently, Kawamura et al. [207] have demonstrated an infrared LED based on an ytterbium complex (ytterbium (dibenzoylemethanato)<sub>3</sub>(bathophenanthroline)). Intense emission was demonstrated around  $1\ \mu\text{m}$  with a threshold voltage of 15 V. Improvements to the device structure by Hong et al. [208] have increased the efficiency of electron injection into the active layer and resulted in a device with a turn-on voltage of 4.5 V.

## 6. Future prospects

Work continues apace on erbium-doped silicon, driven by the enormous potential benefits of silicon-based optoelectronics. Excitation and de-excitation mechanisms in crystalline and amorphous silicon are now relatively well understood, and while the low emission efficiencies remain problematic, the short luminescence lifetime of Er in silicon promises fast directly modulated sources. Recent work on turning the table to produce silicon-based detectors operating at  $1.5\ \mu\text{m}$  and thereby using backtransfer mechanisms to advantage [23] have pointed the way to fast all-silicon photodetectors compatible with existing telecommunications technology.

Despite the wide range of semiconductor materials that have been used to produce erbium-doped LEDs, no device has yet achieved sufficient efficiency to be competitive with existing III–V-based sources. Work therefore continues on pushing quantum efficiency figures up by exploiting such techniques as quantum confinement and photonic nanostructures. Confined systems remain of great interest thanks to the ability to tune the optical response of the host and to utilise quantum confinement effects to optimise both optical and electrical host–rare-earth interactions. Erbium-doped silicon microcavities are in their early days and show much promise; likewise nanostructured and nanocrystalline materials, which exhibit interesting nonlinear optical properties.

Although the EDFA is a technology rapidly approaching maturity, the requirement for ever-higher gain bandwidths is driving research on rare-earth doped fibres in a number of directions. Increasing the bandwidth of erbium-doped fibres through modification of the host is enabling amplification in the  $L$ - and

S-bands, and such amplifiers are beginning to be deployed more widely. Simultaneously, neodymium and praseodymium-doped fluoride fibres are opening up the 1.3  $\mu\text{m}$  region as a serious possibility for use in long-haul telecommunications. Likewise, Tm-doped materials are extending gain into the 1.4  $\mu\text{m}$  region; a development made possible by the production of very low –OH content fibres.

The increased deployment of local-area WDM necessitates the development of cheap planar gain elements. In this field, work continues on the production of planar waveguide devices using silica, fluorides, tellurites, polymers, and chalcogenides. Whilst concentration quenching limits the ultimate gain achievable from doped materials, work on low temperature CVD and careful design of wave guide geometries can help to mitigate these effects.

Wide bandgap materials such as GaN are beginning to make a real contribution to the field of visible emission from rare earths. Multicolour rare-earth doped GaN devices have been demonstrated, but much work remains to be done on understanding luminescence mechanisms and increasing efficiencies. This will remain an important and growing field, and of course this area is of great interest scientifically as well as technologically.

A new application for rare-earth doped optical materials that is beginning to receive a lot of attention is that of optical storage. Work by Maeda has shown that erbium-doped garnets can exhibit an optical bistability that makes them suitable for all-optical memories [209]. Erbium-doped lutetium aluminium garnet (Er-LuAG) and erbium-doped yttrium aluminium garnet (Er-YAG) exhibit a negative nonlinear absorption effect as a result of both ground-state and excited-state absorption mechanisms being present under 1530 nm illumination [210]. Thanks to Stark

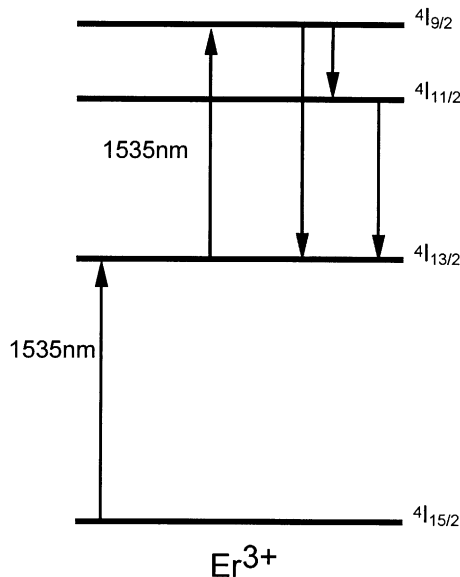


Fig. 16. Processes involved in negative nonlinear absorption in erbium.

splitting, it is possible to populate the  $^4I_{9/2}$  manifold from the  $^4I_{13/2}$  levels by excited state absorption of 1530 nm light. Spontaneous radiative transitions from the  $^4I_{11/2}$  level to the metastable  $^4I_{13/2}$  state can lead to stimulated emission, which can enhance excited state absorption at 1530 nm ( $^4I_{13/2}$  to  $^4I_{9/2}$ ) by increasing the population of the  $^4I_{13/2}$  level. As a result, the degree of absorption at 1.53  $\mu\text{m}$  increases with pump power. The negative nonlinear absorption effect can be employed to greatly increase the degree of modulation for high-gain EDFAs or to produce systems that exhibit optical bistability. Fig. 16 summarises the processes involved. However, the key result is that the optical bistability can occur for very low incident pump powers (of the order of a few  $\text{mW cm}^{-2}$ ). These are promising results from the perspective of producing optical computers.

In conclusion, therefore, the field of rare-earth doped optoelectric materials remains a lively and rapidly developing one. There is a great deal of interesting physics to be investigated, particularly in the area of nanostructured materials, and the needs of technology are constantly pushing forward research into new ways of integrating light emitting materials with existing semiconductor and fibre technology. There remains a strong emphasis on telecommunications compatible wavelengths around 1.5  $\mu\text{m}$ , though there are a number of novel solutions aimed at extending the capabilities of rare-earth doped materials to satisfy the ever-increasing demand for gain bandwidth in this region.

## References

- [1] A. Polman, *Physica B* 300 (2001) 78.
- [2] G.H. Dieke, in: H.M. Crosswhite, H. Crosswhite (Eds.), *Spectra and Energy levels of Rare-Earth Ions in Crystals*, Wiley, New York, 1968.
- [3] P.J. Mears, L. Reekie, I.M. Jauncey, D.N. Payne, *Electronics Letters* 23 (1987) 1026.
- [4] E. Desurvire, R.J. Simpson, P.C. Becker, *Optics Letters* 12 (1987) 888.
- [5] E. Desurvire, *Physics Today* 47 (1994) 20.
- [6] Shibin Jiang (Ed.), *Rare-Earth Doped Materials and Devices IV*, Proceedings of SPIE 3942 (2000).
- [7] Shibin Jiang (Ed.), *Rare-Earth Doped Materials and Devices V*, Proceedings of SPIE 4282 (2001).
- [8] Proceedings of E-MRS symposium on rare earth doped semiconductors Materials Science and Engineering B III (2001) 81.
- [9] C. Brecher, L.A. Riseberg, *Physical Review B* 13 (1976) 81.
- [10] Y.D. Huang, M. Mortier, F. Auzel, *Optical Materials* 15 (2001) 243.
- [11] P.W. Atkins, *Physical Chemistry*, 2nd Edition, Oxford University Press, Oxford, 1983.
- [12] B.R. Judd, *Physical Review* 127 (1962) 750.
- [13] G.S. Ofeldt, *Journal of Chemistry and Physics* 37 (1962) 511.
- [14] E. Desurvire, *Erbium-Doped Amplifiers, Principles and Applications*, Wiley, New York, 1994.
- [15] W. Miniscalco, *IEEE Journal of Lightwave Technology* 9 (1991) 234.
- [16] M.D. Shinn, W.A. Sibley, M.G. Drexhage, R.N. Brown, *Physical Review B* 27 (1983) 6635.
- [17] Th. Förster, *Annales de Physique* 2 (1948) 55.
- [18] D.L. Dexter, *Journal of Chemistry and Physics* 21 (1953) 836.
- [19] A. Polman, *Journal of Applied Physics* 82 (1997) 1.
- [20] S. Coffa, G. Franzò, F. Priolo, *MRS Bulletin* 23 (4) (1998) 25.
- [21] F. Auzel, P. Goldner, *Optical Materials* 16 (2001) 174114.
- [22] J. Laegsgaard, *Physical Review B* 65 (2002) 93.
- [23] N. Hamelin, P.G. Kik, J.F. Suyver, K. Kikoin, A. Polman, A. Schönecker, F.W. Saris, *Journal of Applied Physics* 88 (2000) 5381.

- [24] A. Suchoki, J.M. Langer, *Physical Review B* 39 (1989) 7905.
- [25] G. Franzò, F. Priolo, S. Coffa, *Journal of Luminescence* 80 (1999) 19.
- [26] G. Franzò, S. Coffa, F. Priolo, C. Spinella, *Journal of Applied Physics* 81 (1997) 2784.
- [27] H. Ennen, J. Schneider, G. Pomeranke, A. Axmann, *Applied Physics Letters* 43 (1983) 943.
- [28] H. Ennen, G. Pomeranke, A. Axmann, K. Eisele, W. Haydl, J. Schneider, *Applied Physics Letters* 46 (1985) 381.
- [29] J. Michel, J.L. Benton, R.F. Ferrante, D.C. Jacobson, D.J. Eaglesham, E.A. Fitzgerald, Y.-H. Xie, J.M. Poate, L.C. Kimerling, *Journal of Applied Physics* 70 (1991) 2672.
- [30] S. Scalese, G. Franzò, S. Mirabella, M. Re, A. Terrasi, F. Priolo, E. Rimini, A. Carnera, *Materials Science and Engineering B* 81 (2001) 62.
- [31] S. Coffa, F. Priolo, G. Franzò, V. Bellani, A. Carnera, C. Spinella, *Physical Review B* 48 (1993) 11782.
- [32] J.J. Pradissitto, Ph.D. Thesis, University of London, 1996.
- [33] F. Priolo, S. Coffa, G. Franzò, C. Spinella, A. Carnera, V. Bellani, *Journal of Applied Physics* 74 (1993) 4936.
- [34] J. Palm, F. Gan, B. Zheng, J. Michel, L.C. Kimerling, *Physical Review B* 54 (1996) 17603.
- [35] B. Zheng, J. Michel, F.Y.G. Ren, L.C. Kimerling, D.C. Jacobson, J.M. Poate, *Applied Physics Letters* 64 (1994) 2842.
- [36] G. Franzò, F. Priolo, S. Coffa, A. Polman, A. Carnera, *Applied Physics Letters* 64 (1994) 2235.
- [37] A. Polman, G.N. Van den Hoven, J.S. Custer, R. Serna, P.F.A. Alkemade, *Journal of Applied Physics* 77 (1995) 1256.
- [38] B.J. Pawlak, T. Gregorkiewicz, *Materials Science and Engineering B* 81 (2001) 59.
- [39] M. Needels, M. Schlüter, M. Lannoo, *Physical Review B* 47 (1993) 15533.
- [40] H. Przybylinska, W. Jantsch, Y. Suprun-Belevich, M. Stepihova, L. Palmetshofer, G. Hendorfer, A. Kozanecki, R.J. Wilson, B.J. Sealy, *Physical Review B* 54 (1996) 2532.
- [41] D.L. Adler, D.C. Jacobson, D.J. Eaglesham, M.A. Marcus, J.L. Benton, J.M. Poate, P.H. Citrin, *Applied Physics Letters* 61 (1992) 2181.
- [42] M. Ishii, Y. Komukai, *Applied Physics Letters* 79 (2001) 934.
- [43] V.V. Kveder, E.A. Steinman, S.A. Shevchenko, H.G. Grimmeiss, *Physical Review B* 51 (1995) 10520.
- [44] N.A. Sobolev, O.B. Gusev, E.I. Shek, V.I. Vdovin, T.G. Yugova, A.M. Emel'yanov, *Journal of Luminescence* 80 (1999) 357.
- [45] T. Ostereich, C. Swiatowski, I. Broser, *Applied Physics Letters* 56 (1990) 446.
- [46] I. Yassievich, M. Bresler, O. Gusev, *Journal of Non-Crystalline Solids* 226 (1998) 192.
- [47] J.H. Shin, M.J. Kim, *Journal of Vacuum Science and Technology A* 17 (1999) 3230.
- [48] A.R. Zanatta, F.L. Freire, *Physical Review B* 62 (2000) 2016.
- [49] M.S. Bresler, O.B. Gusev, T.E. Pak, E.I. Terukov, K.D. Tsendin, I.N. Yassievich, *Semiconductors* 33 (1999) 622.
- [50] O.B. Gusev, M.S. Bresler, E.I. Terukov, K.D. Tsendin, I.N. Yassievich, *Journal of Luminescence* 80 (1998) 335.
- [51] V.F. Masterov, F.S. Nasredinov, P.P. Seregin, V.Kh. Kudoyarova, A.N. Kuznetsov, E.I. Terukov, *Applied Physics Letters* 72 (1998) 728.
- [52] I.N. Yassievich, M.S. Bresler, O.B. Gusev, P.E. Pak, K.D. Tsendin, E.I. Terukov, *Materials Science and Engineering B* 81 (2001) 182.
- [53] L.T. Canham, *Applied Physics Letters* 57 (1990) 1046.
- [54] A. Loni, A.J. Simons, T.I. Cox, P.D.J. Calcott, L.T. Canham, *Electronics Letters* 31 (1995) 1288.
- [55] T. Kimura, A. Yokoi, H. Horiguchi, R. Saito, T. Ikoma, A. Sato, *Applied Physics Letters* 65 (1994) 983.
- [56] T. Taskin, S. Gardelis, J.H. Evans, B. Hamilton, A.R. Peaker, *Electronics Letters* 31 (1995) 2132.
- [57] R.T. Collins, P.M. Fauchet, M.A. Tischler, *Physics Today* 50 (1997) 24.
- [58] S. Uekusa, T. Inomata, *Journal of Luminescence* 80 (1999) 339.
- [59] H.A. Lopez, P.M. Fauchet, *Materials Science and Engineering B* 81 (2001) 91.

- [60] R. White, X. Wu, U. Hömmerich, F. Namavar, A.M. Cremins-Costa, Material Research Society Symposium Proceedings 422 (1996) 137.
- [61] W. Wang, H. Isshiki, S. Yugo, R. Saito, T. Kimura, Journal of Luminescence 87–89 (2000) 319.
- [62] T. Kimura, I. Hosokawa, Y. Nishida, T. Dejima, R. Saito, T. Ikoma, Material Research Society Symposium Proceedings 422 (1996) 149.
- [63] J.V. St. John, J.L. Coffey, Y. Chen, R.F. Pinizzotto, Proceedings of the Electrochemical Society 98 (19) (1999) 61.
- [64] J.V. St. John, J.L. Coffey, Y. Chen, R.F. Pinizzotto, Applied Physics Letters 77 (2000) 1635.
- [65] Y. Kanzawa, T. Kageyama, S. Takevka, M. Fujii, S. Hayashi, K. Yamamoto, Solid State Communications 102 (1997) 533.
- [66] M.F. Cerqueira, M.V. Stepihova, J.A. Ferreira, Materials Science and Engineering B 81 (2001) 32.
- [67] S.B. Aldabergenova, M. Albrecht, H.P. Strunk, J. Viner, P.C. Taylor, A.A. Andreev, Materials Science and Engineering B 81 (2001) 29.
- [68] X.W. Zhao, S. Komuro, H. Isshiki, Y. Aoyagi, T. Sugano, Applied Physics Letters 74 (1999) 120.
- [69] A.A. Dukin, N.A. Feokistov, V.G. Golubev, A.V. Medvedev, A.B. Pevstov, A.V. Sel'kin, Applied Physics Letters 77 (2000) 3009.
- [70] H.A. Lopez, P.M. Fauchet, Physica Status Solidi A 182 (2000) 413.
- [71] Y. Zhou, P.A. Snow, P.St.J. Russell, Materials Science and Engineering B 81 (2001) 40.
- [72] E.F. Schubert, A.M. Vredenberg, N.E.J. Hunt, Y.H. Wong, P.C. Becker, M.J. Poate, D.C. Jacobson, L.C. Feldman, G.J. Zyzdik, Applied Physics Letters 61 (1992) 1381.
- [73] M. Lipson, T. Chen, K. Chen, X. Duan, L.C. Kimerling, Materials Science and Engineering B 81 (2001) 36.
- [74] M. Lipson, L.C. Kimerling, Applied Physics Letters 77 (2000) 1150.
- [75] H.A. Lopez, P.M. Fauchet, Applied Physics Letters 77 (2000) 3704.
- [76] M.Q. Huda, A.R. Peaker, J.H. Evans, D.C. Houghton, W.P. Gillin, Electronics Letters 33 (1997) 1182.
- [77] S.J. Chang, D.K. Nayak, Y. Shiraki, Journal of Applied Physics 83 (1998) 1426.
- [78] E. Neufeld, A. Sticht, K. Brunner, G. Abstreiter, H. Holzbrecher, H. Bay, Ch. Buchal, Applied Physics Letters 71 (1997) 3129.
- [79] K.D. Vernon-Parry, I.D. Hawkins, J.H. Evans-Freeman, P. Dawson, A.R. Peaker, Material Science and Engineering B 81 (2001) 164.
- [80] C.-X. Du, W.-X. Ni, K.B. Joëlsson, F. Duteil, Göran, Journal of Luminescence 80 (1999) 329.
- [81] H. Ennen, J. Schneider, Journal of Electronic Materials A 14 (1985) 115.
- [82] V.V. Ushakov, A.A. Gippius, V.A. Dravlin, A.V. Spitsyn, Soviet Physics—Semiconductors 16 (1982) 723.
- [83] R.S. Smith, H.D. Muller, H. Ennen, P. Wennekers, M. Maier, Applied Physics Letters 50 (1987) 49.
- [84] F. Bantien, E. Bauser, J. Weber, Journal of Applied Physics 61 (1987) 2803.
- [85] A.R. Zanatta, Applied Physics Letters 75 (1999) 3279.
- [86] K. Takahei, R.A. Hogg, A. Taguchi, Materials Research Society Symposium Proceedings 422 (1996) 267.
- [87] D. Haase, A. Dörnen, K. Takahei, A. Taguchi, Materials Research Society Symposium Proceedings 422 (1996) 179.
- [88] T. Benyattou, D. Seghier, G. Brémond, S. Moneger, A. Kalboussi, G. Marrakchi, G. Guillot, C. Lhomer, B. Lambert, Y. Toudic, A. Le Corre, Materials Research Society Symposium Proceedings 301 (1993) 163.
- [89] A.R. Peaker, H. Efeoglu, J.M. Langer, A.C. Wright, I. Poole, K.E. Singer, Materials Research Society Symposium Proceedings 301 (1993) 337.
- [90] I. Poole, K.E. Singer, A.R. Peaker, Journal of Crystal Growth 121 (1992) 121.
- [91] A.R. Peaker, F. Coppinger, H. Efeoglu, J.H. Evans-Freeman, D.K. Maude, J.C. Portal, P. Rutter, K.E. Singer, A. Scholes, A.C. Wright, Materials Science Forum, Vol. 258(2), 1997, p. 1551.
- [92] K.E. Singer, P. Rutter, A.R. Peaker, A.C. Wright, Applied Physics Letters 64 (1994) 707.
- [93] M.R. Bennett, K.E. Singer, A.C. Wright, Z.H. Jafri, Materials Research Society Symposium Proceedings 422 (1996) 29.

- [94] R.L. Maltez, Z. Liliental-Weber, J. Washburn, M. Behar, P.B. Klein, P. Specht, E.R. Weber, *Journal of Applied Physics* 85 (1999) 1105.
- [95] K. Takahei, A. Taguchi, in: G. Davies, G. Deleo, M. Stavola (Eds.), *Defects in Semiconductors*, Vol. 16, Trans Tech Publications Ltd., Zurich, 1992, p. 641.
- [96] A. Taguchi, K. Takahei, J. Nakata, *Materials Research Society Symposium Proceedings* 301 (1993) 139.
- [97] G.M. Ford, B.W. Wessels, *Materials Research Society Symposium Proceedings* 422 (1996) 345.
- [98] S.J. Chang, *Materials Research Society Symposium Proceedings* 422 (1996) 351.
- [99] S.N. Mohammad, H. Morkoç, *Progress in Quantum Electronics* 20 (1996) 361.
- [100] P.N. Favennec, H. L'Haridon, M. Salvi, D. Muotonnet, Y. Le Guillo, *Electronics Letters* 25 (1989) 718.
- [101] T.M. Levin, A.P. Young, J. Schafer, L.J. Brillson, J.D. Mackenzie, C.R. Abernathy, *Journal of Vacuum Science Technology A* 17 (1999) 3437.
- [102] A.J. Steckl, J.M. Zavada, *MRS Bulletin* 24 (9) (1999) 33.
- [103] H. Lozykowski, W.M. Jadwisieczack, I.M. Brown, *Journal of Applied Physics* 88 (2000) 210.
- [104] R. Birkhahn, R. Hudgins, D.S. Lee, A.J. Steckl, A. Saleh, R.G. Wilson, J.M. Zavada, *MRS Internet Journal of Nitride Semiconductor Research* 4S1 (1999) G3.10.
- [105] A.J. Steckl, R. Birkhahn, *Applied Physics Letters* 73 (1998) 2143.
- [106] L.C. Chao, B.K. Lee, C.J. Chi, J. Cheng, I. Chyr, A.J. Steckl, *Applied Physics Letters* 75 (1999) 1833.
- [107] R. Birkhahn, M. Garter, A.J. Steckl, *Applied Physics Letters* 74 (1999) 2161.
- [108] J. Heikenfeld, M. Garter, D.S. Lee, R. Birkhahn, A.J. Steckl, *Applied Physics Letters* 74 (1998) 1129.
- [109] H. Lozykowski, W.M. Jadwisieczack, I.M. Brown, *Applied Physics Letters* 75 (1999) 1189.
- [110] A.J. Steckl, M. Garter, D.S. Lee, J. Heikenfeld, R. Birkhahn, *Applied Physics Letters* 75 (1999) 2184.
- [111] S. Kim, S.J. Rhee, J.O. White, A.M. Mitofsky, X. Li, G.C. Papen, J.J. Coleman, S.G. Bishop, *Materials Science and Engineering B* 81 (2001) 136.
- [112] L.C. Chao, A.J. Steckl, *Applied Physics Letters* 74 (1999) 2364.
- [113] J.M. Zavada, C.J. Ellis, J.Y. Lin, H.X. Jiang, J.T. Seo, U. Hömmerich, M. Thaik, R.G. Wilson, P.A. Grudowski, R.D. Dupuis, *Materials Science and Engineering* 81 (2001) 127.
- [114] U. Hömmerich, J.T. Seo, C.R. Abernathy, A.J. Steckl, J.M. Zavada, *Materials Science and Engineering B* 81 (2001) 116.
- [115] S. Kim, S.J. Rhee, X. Li, J.J. Coleman, S.G. Bishop, *Applied Physics Letters* 76 (2000) 2403.
- [116] S. Kim, S.J. Rhee, X. Li, J.J. Coleman, S.G. Bishop, *Journal of Electronic Materials* 28 (1999) 266.
- [117] R.G. Wilson, R.N. Schwartz, C.R. Abernathy, S.J. Pearton, N. Newman, M. Rubin, T. Fu, J.M. Zavada, *Applied Physics Letters* 65 (1994) 992.
- [118] M. Thaik, U. Hömmerich, R.N. Schwartz, R.G. Wilson, J.M. Zavada, *Applied Physics Letters* 71 (1997) 2641.
- [119] H. Shen, J. Pamulapati, M. Taysing, M.C. Wood, R.T. Lareau, M.H. Ervin, J.D. Mackenzie, C.R. Abernathy, S.J. Pearton, F. Ren, J.M. Zavada, *Solid State Electronics* 43 (1999) 1231.
- [120] J.T. Torvik, R.J. Fuerstein, C.H. Qiu, J.I. Pankove, F. Namavar, *Journal of Applied Physics* 82 (1997) 1824.
- [121] S. Kim, S.J. Rhee, X. Li, J.J. Coleman, S.G. Bishop, P.B. Klein, *Journal of Electronic Materials* 27 (1998) 246.
- [122] C.H. Qiu, M.W. Leksono, J.I. Pankove, J.T. Torvik, R.J. Fuerstein, F. Namavar, *Applied Physics Letters* 66 (1995) 562.
- [123] M. Overberg, C.R. Abernathy, J.D. MacKenzie, S.J. Pearton, R.G. Wilson, J.M. Zavada, *Materials Science and Engineering B* 81 (2001) 121.
- [124] W.J. Choyke, R.P. Devaty, L.L. Clemen, M. Yoganathan, G. Pensl, Ch. Hassler, *Applied Physics Letters* 65 (1994) 1668.

- [125] M. Yoganathan, W.J. Choyke, R.P. Devaty, G. Pensl, J.A. Edmond, Material Research Society Symposium Proceedings 422 (1996) 339.
- [126] M. Dejneka, B. Samson, MRS Bulletin 24 (1999) 39.
- [127] H. Ono, M. Yamada, T. Kanamori, Y. Ohishi, IEEE Photonics Technology Letters 9 (1997) 596.
- [128] B.-H. Choi, H.-H. Park, M. Chu, S.K. Kim, IEEE Photonics Technology Letters 13 (2001) 109.
- [129] M.A. Mahdi, F.R. Mahamd Adikan, P. Poopalan, S. Selvakennedy, H. Ahmad, Optics Communications 187 (2001) 389.
- [130] I. Massarek, Ph.D. Thesis, University of London, 1994.
- [131] N. Can, P.D. Townsend, D.E. Hole, H.V. Snelling, J.M. Ballesteros, C.N. Afonso, Journal of Applied Physics 78 (1995) 6737.
- [132] T. Kitagawa, F. Bilodeau, B. Malo, S. Theriault, J. Albert, D.C. Jihson, K.O. Hill, K. Hattori, Y. Hibino, Electronics Letters 30 (1994) 1311.
- [133] Q. Xiang, Y. Zhou, B.S. Ooi, Y.L. Lam, Y.C. Chan, C.H. Kam, Thin Solid Films 370 (2000) 243.
- [134] E. Snoeks, P.J. Kik, A. Polman, Optical Materials 5 (1996) 159.
- [135] D.J. DiMaria, J.R. Kirtley, E.J. Pakulis, D.W. Dong, T.S. Kuan, F.L. Pesavento, T.N. Theis, J.A. Cutro, S.D. Brorson, Journal of Applied Physics 56 (1984) 401.
- [136] T. Shimizu-Iwayama, K. Fujita, S. Nakao, K. Saitoh, T. Fujita, N. Itoh, Journal of Applied Physics 75 (1994) 7779.
- [137] A.J. Kenyon, P.F. Trwoga, C.W. Pitt, G. Rehm, Journal of Applied Physics 79 (1996) 9291.
- [138] A.J. Kenyon, P.F. Trwoga, C.W. Pitt, G. Rehm, Applied Physics Letters 73 (1998) 523.
- [139] A.J. Kenyon, P.F. Trwoga, M. Federighi, C.W. Pitt, Journal of Physics: Condensed Matter 6 (1994) L319.
- [140] M. Fujii, M. Yoshida, Y. Kanzawa, S. Hayashi, K. Yamamoto, Applied Physics Letters 71 (1997) 1198.
- [141] J.H. Shin, M. Kim, S. Seo, C. Lee, Applied Physics Letters 72 (1998) 1092.
- [142] G. Franzò, V. Vinciguerra, F. Priolo, Applied Physics A 69 (1999) 3.
- [143] A.J. Kenyon, C.E. Chryssou, C.W. Pitt, T. Shimizu-Iwayama, D.E. Hole, N. Sharma, C.J. Humphreys, Journal of Applied Physics 91 (2002) 367.
- [144] A.J. Kenyon, C.E. Chryssou, C.W. Pitt, in: Shibin Jiang (Ed.), Rare-Earth-Doped Materials and Devices V, Proceedings of the SPIE 4282 (2001) 185.
- [145] A.J. Kenyon, C.E. Chryssou, C.W. Pitt, T. Shimizu-Iwayama, D.E. Hole, N. Sharma, C.J. Humphrey, Materials Science and Engineering B 81 (2001) 19.
- [146] H.-K. Han, S.-Y. Seo, J.H. Shin, Applied Physics Letters 79 (2001) 4568.
- [147] G.Z. Ran, Y. Chen, W.C. Qin, J.S. Fu, Z.C. Ma, W.H. Zong, H. Lu, J. Qin, G.G. Qin, Journal of Applied Physics 90 (2001) 5835.
- [148] Y. Chen, G.Z. Ran, L. Dai, B.R. Zhang, G.G. Qin, Z.C. Ma, W.H. Zong, Applied Physics Letters 80 (2002) 2496.
- [149] S. Wang, S. Coffa, R. Carius, Ch. Buchal, Materials Science and Engineering B 81 (2001) 102.
- [150] G.N. van den Hoven, E. Snoeks, A. Polman, C. van Dam, J.W.M. van Uffelen, M.K. Smit, Applied Physics Letters 79 (1996) 1258.
- [151] G.N. van den Hoven, E. Snoeks, A. Polman, J.W.M. van Uffelen, Y.S. Oei, M.K. Smit, Applied Physics Letters 62 (1993) 3065.
- [152] C.E. Chryssou, C.W. Pitt, IEEE Journal of Quantum Electronics 34 (1998) 282.
- [153] G.N. van den Hoven, R.J. Koper, A. Polman, C. van Dam, J.W.M. van Uffelen, M.K. Smit, Applied Physics Letters 68 (1996) 1886.
- [154] C.E. Chryssou, C.W. Pitt, P.J. Chandler, D.E. Hole, IEE Proceedings of Optoelectronics 145 (1998) 325.
- [155] M. Federighi, IEEE Journal of Quantum Electronics 30 (1994) 2127.
- [156] F. Di Pasquale, C.E. Chryssou, F. Di Pasquale, C.W. Pitt, IEEE Journal of Lightwave Technology 19 (2001) 345.
- [157] J.A. Lázaro, J.A. Vallés, M.A. Rebolledo, IEEE Journal of Quantum Electronics 35 (1998) 827.
- [158] J. Amin, B. Duassardier, T. Schweizer, M. Hempsted, Journal of Luminescence 69 (1996) 17.

- [159] F. Caccavale, C. Sada, F. Segato, B. Allieri, L.E. Depero, L. Sangaletti, V.A. Fedorov, Yu.N. Korkishko, T.V. Morozova, *Journal of Non-Crystalline Solids* 280 (2001) 156.
- [160] B. Herreros, G. Lifante, F. Cusso, J.A. Sanz, A. Kling, J.C. Soares, M.F. da Silva, P.D. Townsend, P.J. Chandler, *Journal of Physics: Condensed Matter* 10 (1998) 3275.
- [161] R. Brinkmann, I. Baumann, M. Dinand, W. Sohler, H. Suche, *IEEE Journal of Quantum Electronics* 30 (1994) 2356.
- [162] I. Baumann, R. Brinkmann, M. Dinand, W. Sohler, S. Westenhöfer, *IEEE Journal of Quantum Electronics* 32 (1996) 1695.
- [163] C. Mignotte, *Nuclear Instrumentation and Methods in Physics Research B* 187 (2002) 95.
- [164] L. Rebouta, M.F. da Silva, J.C. Soares, J.A. Sanz-Garcia, E. Dieguez, F. Agulló-Lopez, *Nuclear Instrumentation and Methods in Physics Research B* 64 (1992) 189.
- [165] T. Gög, M. Griebenow, G. Materlik, *Physics Letters A* 181 (1993) 417.
- [166] D.M. Gill, J.C. Wright, L. McCaughan, *Applied Physics Letters* 64 (1994) 2483.
- [167] C. Mignotte, *Applied Surface Science* 181 (2001) 11.
- [168] S. Tanabe, in: Shibin Jiang (Ed.), *Rare-Earth Doped Materials and Devices V*, Proceedings of the SPIE 4282 (2001) 85.
- [169] P.W. France, M.G. Drexhage, J.M. Parker, M.W. Moore, S.F. Carter, J.V. Wright, *Fluoride Glass Optical Fibres*, Blackie, London, 1990.
- [170] R. Scheps, *Progress in Quantum Electronics* 20 (1996) 271.
- [171] O. Svelto, *Principles of Lasers*, 4th Edition, Plenum Press, New York, 1998.
- [172] V.K. Bogdanov, W.E.K. Gibbs, D.J. Booth, J.S. Javorniczky, P.J. Newman, D.R. MacFarlane, *Journal of Non-Crystalline Solids* 256 & 257 (1999) 288.
- [173] Y. Nishida, M. Yamada, T. Kanamori, K. Kobayashi, J. Temmyo, S. Sudo, Y. Ohishi, *IEEE Journal of Quantum Electronics* 34 (1998) 1332.
- [174] V. Morin, E. Taufflieb, *IEEE Journal of Selected Topics in Quantum Electronics* 3 (1997) 1112.
- [175] M. Braglia, C. Bruschi, G. Dai, J. Kraus, S. Mosso, C. Meneghini, A. Balerna, F. Boshnerini, S. Pascarelli, C. Lamberti, *Journal of Non-Crystalline Solids* 256 & 257 (1999) 83.
- [176] J.-L. Adam, J.-L. Doualan, L. Griscom, S. Girard, R. Moncorgé, *Journal of Non-Crystalline Solids* 256 & 257 (1999) 276.
- [177] S. Ronchin, R. Rolli, M. Montagna, C. Duverger, V. Tikhomirov, A. Jha, M. Ferrari, G.C. Righini, S. Pelli, M. Fossi, *Journal of Non-Crystalline Solids* 284 (2001) 243.
- [178] D.R. MacFarlane, J. Javorniczky, P.J. Newman, D.J. Booth, *Journal of Non-Crystalline Solids* 256 & 257 (1999) 366.
- [179] P. Santa-Cruz, D. Morin, J. Dexpert-Ghys, A. Sadoc, F. Glas, F. Auzel, *Journal of Non-Crystalline Solids* 190 (1995) 238.
- [180] M. Mortier, F. Auzel, *Journal of Non-Crystalline Solids* 256&257 (1999) 362.
- [181] G. Zhang, J. Jiang, M. Poulain, *Journal of Non-Crystalline Solids* 221 (1997) 78.
- [182] B. Cole, L.B. Shaw, P.C. Pureza, R. Mossadegh, J.S. Sanghera, I.D. Aggarwal, *Journal of Non-Crystalline Solids* 256 & 257 (1999) 253.
- [183] J. Fick, É.J. Knystautas, A. Villeneuve, F. Schiettekatte, S. Roorda, K.A. Richardson, *Journal of Non-Crystalline Solids* 272 (2000) 200.
- [184] S.Q. Gu, S. Ramachandran, E.E. Reuter, D.A. Turnbull, J.T. Verdeyen, S.G. Bishop, *Journal of Applied Physics* 77 (1995) 3365.
- [185] C. Meneghini, J.F. Viens, A. Villeneuve, É.J. Knystautas, M.A. Duguay, K.A. Richardson, *Journal of the Optical Society of America B* 15 (1998) 1305.
- [186] J.S. Sanghera, I.D. Aggarwal, *Journal of Non-Crystalline Solids* 256 & 257 (1999) 6.
- [187] C.C. Ye, D.W. Hewak, M. Hempstead, B.N. Samson, D.N. Payne, *Journal of Non-Crystalline Solids* 208 (1996) 56.
- [188] K. Itoh, H. Yanagita, H. Tawarayama, K. Yamanaka, E. Ishikawa, K. Okada, H. Aoki, Y. Matsumoto, A. Shirakawa, Y. Matsuoka, H. Toratani, *Journal of Non-Crystalline Solids* 256 & 257 (1999) 1.
- [189] D.W. Hewak, B.N. Samson, J.A. Medeiros Neto, R.I. Laming, D.N. Payne, *Electronics Letters* 30 (1994) 968.

- [190] R. Rolli, A. Chiasera, M. Montagna, E. Moser, S. Ronchin, S. Pelli, G.C. Ringhini, A. Jha, V.K. Tikhomirov, S.A. Tikhomirova, C. Diverger, P. Galinetto, M. Ferrari, in: Shibin Jiang (Ed.), Rare-Earth Doped Materials and Devices V, Proceedings of SPIE 4282 (2001) 109.
- [191] C.E. Chryssou, F. Di Pasquale, C.W. Pitt, IEEE Journal of Selected Topics in Quantum Electronics 6 (2000) 114.
- [192] A.P. Lopez-Barbero, W.A. Arellano-Espinoza, H.L. Fragnito, H.E. Hernandez-Figueroa, Microwave Optical Technology Letters 25 (2000) 103.
- [193] M. Yamada, A. Mori, K. Kobayashi, P. Ono, T. Kanamori, K. Oikawa, Y. Nishida, Y. Ohishi, IEEE Photonics Technology Letters 10 (1998) 1244.
- [194] C.E. Chryssou, Optics Communications 184 (2000) 375.
- [195] H. Nii, K. Ozaki, M. Herren, M. Morita, Journal of Luminescence 76 & 77 (1998) 116.
- [196] A. Narazaki, K. Tanaka, K. Hirao, N. Soga, Journal of Applied Physics 85 (1999) 2046.
- [197] Y. Hu, S. Jiang, G. Sorbello, T. Luo, Y. Ding, B.-C. Hwang, J.-H. Kim, H.-J. Seo, N. Peyhambarian, in: Shibin Jiang (Ed.), Rare-Earth Doped Materials and Devices V, Proceedings of the SPIE 4282 (2001) 57.
- [198] A. Mori, Y. Oshishi, S. Sudo, Electronics Letters 33 (1997) 863.
- [199] Y. Ding, S. Jiang, T. Luo, Y. Hu, N. Peyhambarian, in: Shibin Jiang (Ed.), Rare-Earth Doped Materials and Devices V, Proceedings of the SPIE 4282 (2001) 23.
- [200] L.H. Sloof, A. van Blaaderen, A. Polman, G.A. Hebbink, S.I. Klink, F.C.J.M. Van Veggel, D.N. Reinholdt, J.W. Hofstraat, Journal of Applied Physics 91 (2002) 3955.
- [201] R.T. Chen, M. Lee, S. Natarajan, C. Lin, Z.Z. Ho, D. Robinson, IEEE Photonics Technology Letters 5 (1993) 1328.
- [202] G. Karve, B. Bihari, R.T. Chen, Applied Physics Letters 77 (2000) 1253.
- [203] D. Oh, N. Song, J.-J. Kim, in: Shibin Jiang (Ed.), Rare-Earth Doped Materials and Devices V, Proceedings of the SPIE 4282 (2001) 1.
- [204] G. Karve, B. Bihari, R.T. Chen, in: Shibin Jiang (Ed.), Rare-Earth Doped Materials and Devices V, Proceedings of the SPIE 4282 (2001) 16.
- [205] N.V. Gaponenko, O.V. Segeev, V.E. Borisenko, J.C. Pivin, P. Skeldon, G.E. Thompson, B. Hamilton, J. Misiewicz, L. Bryja, R. Kudrawiec, A.P. Stupak, E.A. Stepanova, Materials Science and Engineering B 81 (2001) 191.
- [206] L.H. Sloof, A. Polman, M.P. Oude Wolders, F.C.J.M. van Veggel, D.N. Reinholdt, J.W. Hofstraat, Journal of Applied Physics 83 (1998) 497.
- [207] Y. Kawamura, Y. Wada, M. Iwamuro, T. Kitmaura, S. Yanagida, Chemistry Letters 3 (2000) 280.
- [208] Z.R. Hong, C.J. Liang, R.G. Li, D. Zhao, D. Fan, W.L. Li, Thin Solid Films 391 (2001) 122.
- [209] Y. Maeda, Materials Science and Engineering B 81 (2001) 174.
- [210] Y. Maeda, Y. Matsuoka, Applied Physics Letters 76 (2000) 3504.